THE FLORIDA STATE UNIVERSITY

COLLEGE OF ARTS AND SCIENCES

LOW-FREQUENCY VARIATIONS OF THE SEA BREEZE IN FLORIDA

By

LAUREN MOELLER

A Thesis submitted to the
Department of Earth, Ocean, and Atmospheric Science
in partial fulfillment of the
requirements for the degree of
Master of Science

Degree Awarded:
Summer Semester, 2011

The members of the committee approve the thesis of Lauren Moeller defended on April 28, 2011.

_____
Vasubandhu Misra
Professor Directing Thesis

_____
James J. O'Brien
Professor Co-Directing Thesis

_____
Henry Fuelberg
Committee Member

_____
Mark Bourassa
Committee Member

The Graduate School has verified and approved the above-named committee

My thesis and my work are dedicated to my wonderful parents, Larry and Kim, my sisters Kayla and Jenna, my brother Brandon, and most of all, my support and love, my fiancé Chris.

ACKNOWLEDGEMENTS

First of all I would like to thank Dr. Vasu Misra for accepting me as one of his students here at FSU, and giving me the opportunity to do this work. He has continually pushed me to do the best that I can, and I would not have accomplished as much as I have without his direction and advice.

I would also like to thank Dr. Mark Bourassa, Dr. Henry Fuelberg (HEF), and especially Dr. James J. O'Brien for serving on my committee. Your advice and guidance were extremely helpful from the get-go, and my work here has improved due to your thoughtful contributions.

Along with the committee I would like to thank Dr. Steven Chan and Dr. Lydia Stefanova for their guidance and support, and for helping me through any scripting trouble.

Next I want to thank my family for their continuous support even when they were hundreds of miles away. You guys believed in me during the toughest of times, and this could not have happened without you!

My friends have also been an invaluable support during my time here at FSU. An extra special shout-out goes to those at COAPS and those in Dr. Misra's lab. You guys have made these last two years some of the best in my life, and whether it was a shoulder to cry on or some great advice, you all had it ready. Thank you!

Finally, I want to thank my fiancé Chris for his love and support throughout my graduate school career. There are no words to describe my gratitude for all that you do for me.

TABLE OF CONTENTS

LIST OF TABLES

LIST OF FIGURES

ABSTRACT

The variations in the sea breeze are examined both diurnally and interannually along the panhandle of Florida during the boreal summer season. A climatology of sea breeze cross sections is calculated eight times daily between the years 1979 and 2001 to examine diurnal differences. The cross sections are created using very high resolution dynamically downscaled analyses from the NCEP-DOE (R2) and the ECMWF ERA-40 for the southeast U.S. The high resolution downscaled product is validated with other independent observations to show fidelity. Results from these diurnal analyses show that the sea breeze and precipitation peak at 4:00 p.m.

The interannual variability of the sea breeze is examined with respect to the Atlantic Warm Pool (AWP). Composites consisting of Climate Prediction Center (CPC) precipitation observations are created based on the size of the AWP. These composites show that the strongest low-frequency signal is a negative anomaly along the panhandle. Therefore, model composite cross sections are primarily along the 30.5°N latitude. The cause of the negative anomaly is related to the subtropical high, which undergoes an eastward shift and a decrease in intensity for large AWP years. These changes in the subtropical high lead to a more cyclonic large-scale low-level flow for large AWP years as Sverdrup vorticity balance indicates. This study finds that this synoptic flow pattern will suppress the sea breeze circulation and lessen precipitation amounts over the panhandle region.

CHAPTER ONE

INTRODUCTION

1.1 Objective and Motivation

Although the sea breeze phenomenon is well documented previous studies have often examined sea breezes as individual events, or they have focused on the disparities of the sea breeze circulation that can occur daily. Relatively little attention has been given to variations of the sea breeze on larger time scales. The purpose of this study is to determine whether there are interannual variations of the sea breeze in Florida, and if they do, to examine a possible cause of these variations. The hypothesis is that the sea breeze does have low-frequency variations. These low-frequency variations are examined with respect to changes in the Atlantic Warm Pool (AWP), a topic of interest in the past decade; most studies published on the AWP have occurred since 2001. The findings of this study identify another extensive teleconnection associated with the AWP (Wang and Enfield 2001; Wang et al. 2006; Wang et al. 2008). In addition, determining the low-frequency variation of the sea breeze in Florida will assist the agricultural community and long-range forecasting decisions. Carter (2003) stressed the importance of low frequency variability to the agricultural community in the Southeast. Regional models produce differing results on the timing of the maximum and minimum precipitation (as well as the amount) in a given region. Therefore it is important to establish the teleconnection between the interannually fluctuating AWP and diurnal variability of this region; this knowledge will then drive to improve other models (Carter 2003). Forecasters will also benefit from this knowledge (Powell and Rinard 1998).

1.2 Background

1.2.1 Definition of the Sea Breeze

The sea breeze is part of a thermally direct circulation that exists because of differential heating between the land and the water (Biggs and Graves 1962; Simpson 1994). Temperatures over land increase and decrease more dramatically than those over the water; a pressure gradient at the surface is created since higher pressure exists over the water surface during the daytime. This process induces a flow from higher pressure over the water to relatively lower pressure over land, which is known as a sea breeze (Fig. 1.1). A pressure gradient of the opposite direction

exists aloft and induces a flow in the opposite direction, completing the circulation. The opposite occurs at night when a land breeze develops; however, the land breeze is less prominent than its daytime counterpart (Mak and Walsh 1976). The thermal circulation is also more prominent during the summer in the Northern Hemisphere because the temperature gradient between the land and water is greatest (Simpson 1994).

Sea breezes are especially important during Florida summers (Pielke 1974) because they are responsible for the precipitation that is critical to agricultural interests. Pielke's 1974 study was one of the first to use a 3D model to simulate the sea breeze along the Florida peninsula; prior studies (Estoque 1962; Hsu 1970; Neumann and Mahrer 1971) used a 2D theoretical model. The 3D model showed two sea breezes forming, one along each coast of the Florida peninsula. Pielke juxtaposed vertical velocity predictions and composite radar reflectivities for multiple days and found that on synoptically quiescent days during the summer months, the sea breeze was the main instigator of convection in Florida.

1.2.2 Synoptic Scale Influences

Even though a sea breeze is a mesoscale feature, it is often influenced by forcing that exists on the synoptic scale. An example of this synoptic influence is shown by Lopez et al. (1984), who classified the amount of convective coverage into four categories on the basis of radar data for each day in South Florida. The average synoptic pattern was then produced for each category by using soundings and maps. They discovered that the synoptic flow regimes' influence on the sea breeze circulations was the greatest contributor to the differences between the convective categories. In a follow-up study, Blanchard and Lopez (1985) showed that the patterns of convection on the radar were closely related to the synoptic wind field.

Arritt (1993) demonstrated how the background synoptic wind flow influences the sea breeze by simulating, in a 2D model, different ambient offshore and onshore flows. The strength and direction of the ambient flow greatly influenced the inland penetration of the sea breeze. For example, if light to moderate offshore flow existed, the sea breeze front was enhanced and able to penetrate inland. Arritt also discovered that if the offshore flow was too strong, the sea breeze could develop but would stay mainly offshore. Not only is the inland penetration affected but the ambient wind also affects the strength of the sea breeze. The offshore and onshore flow can weaken or strengthen the temperature gradient between the land and sea; the temperature gradient is directly linked to sea breeze strength (Arritt 1993). Background synoptic winds also

influence the advection of moisture, as demonstrated by Fuelberg and Biggar (1994) when they examined the convection occurring along the Florida panhandle.

Since the synoptic flow has such an influence on the sea breeze, an analysis of the prevailing synoptic conditions is necessary for sea breeze forecasting. Powell and Rinard (1996) described the process of forecasting the sea breeze and convection during the 1996 Summer Olympic Games in Atlanta, Georgia. Figure 1.2, from Powell and Rinard (1996), shows the different synoptic regimes that occurred during the summer of 1996 with respect to the Bermuda high (also known as the North Atlantic subtropical high) and pressure systems moving through the United States. Each regime resulted in a different background flow in the forecast region of Georgia. Additional studies also concluded that the location of the Bermuda high influences the formation of the sea breeze (Lopez et al. 1984; Blanchard and Lopez 1985). Miller and Keim (2003) determined which synoptic patterns were conducive for sea breeze formation in an attempt to develop a forecasting product for sea breezes.

The synoptic scale influences on sea breezes have been well documented. The present study argues that since the synoptic flow varies interannually, low-frequency variations exist in the Florida sea breeze. These low-frequency variations will be analyzed in the context of the AWP.

1.2.3 The Atlantic Warm Pool

The AWP was defined in Wang and Enfield (2001) as a region in the Gulf of Mexico, the Caribbean Sea, and the western tropical North Atlantic that has sea temperatures of at least 28.5°C. The size of the AWP fluctuates from year to year, as shown in a schematic by Wang et al. (2006) (Fig. 1.3). During large AWP years, the 28.5°C isotherm dips east and south to reach into the tropical North Atlantic, and during small AWP years the AWP is confined to the Gulf of Mexico and parts of the Caribbean Sea. On average, the large AWP is three times larger than the small AWP. Climatologically, the AWP is largest during the later part of the warm season (August, October, November; Wang et al. 2006), but the AWP also is distinguishable during June and July. Wang et al. (2006) also noted that the variability in the AWP size was unrelated to the El-Niño Southern Oscillation (ENSO) two-thirds of the time, but ENSO can influence the AWP. However, this study is limited to the AWP effects on the sea breeze and does not address the possible impacts of ENSO on the AWP.

Various teleconnections have been discussed in the literature in response to the implications of the different sizes of the AWP (Wang et al. 2006; Wang et al. 2008). During large AWP years, the pressure falls in the Caribbean region and Mexico and the precipitation increases. Wind speeds decrease during large AWP years over the Gulf of Mexico, thus creating a weaker Great Plains low-level jet (GPLLJ). Therefore, an environment is created for reduced precipitation over the Great Plains region due to lack of transport. Research has also related the size of the AWP to Atlantic hurricane activity (Wang et al. 2006; Wang and Lee 2007; Wang et al. 2008). During large AWP years the Caribbean low-level jet (CLLJ) weakens because of the position of the Bermuda high, reducing the vertical wind shear over the Caribbean region. In conjunction with lower values of vertical wind shear, warmer waters extend farther to the east and south than they normally would during small AWP years. There is increased hurricane activity in the Atlantic basin during large AWP years because of the lower wind shear and warmer waters (Wang et al. 2006, Wang and Lee 2007, Wang et al. 2008).

This study focuses on AWP teleconnections and how they modulate the sea breeze in Florida on an interannual time scale. The remainder of this paper is organized as follows: the model runs, verification data, and methodology are described in chapter two; the model results are presented and discussed in depth in chapter three; and conclusions are stated in chapter four.

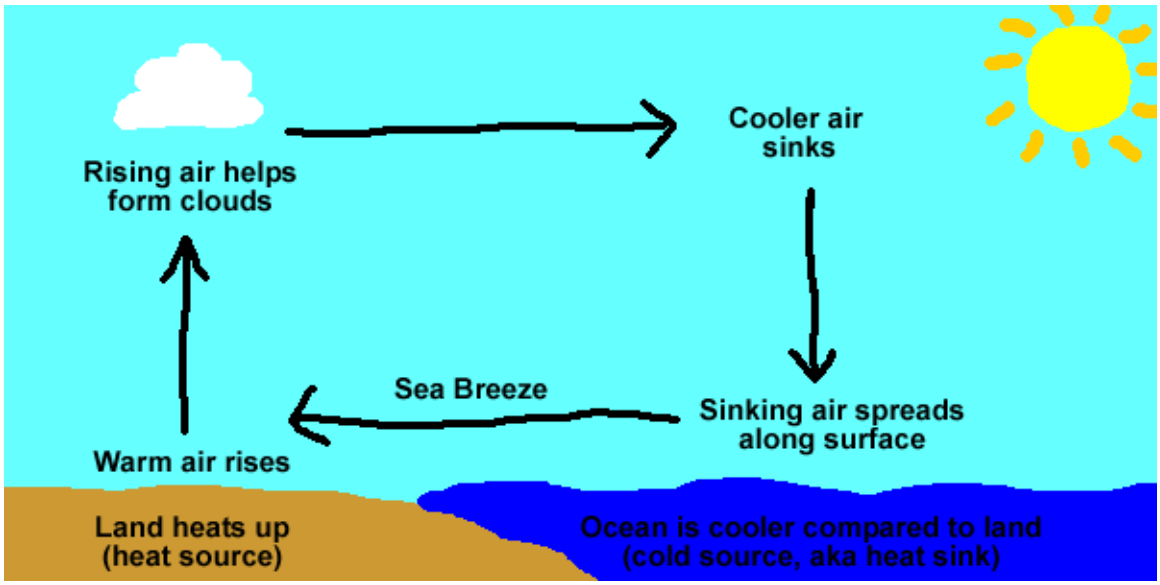

Fig. 1.1. Schematic from the National Weather Service office in Honolulu (http://www.prh.noaa.gov/hnl/kids/activities.php) showing the daytime component of the thermal circulation, with arrows denoting the direction of the flow. The ocean is denoted by dark blue and the land by brown. The arrow on the top of the circulation is part of the return flow that completes the circulation

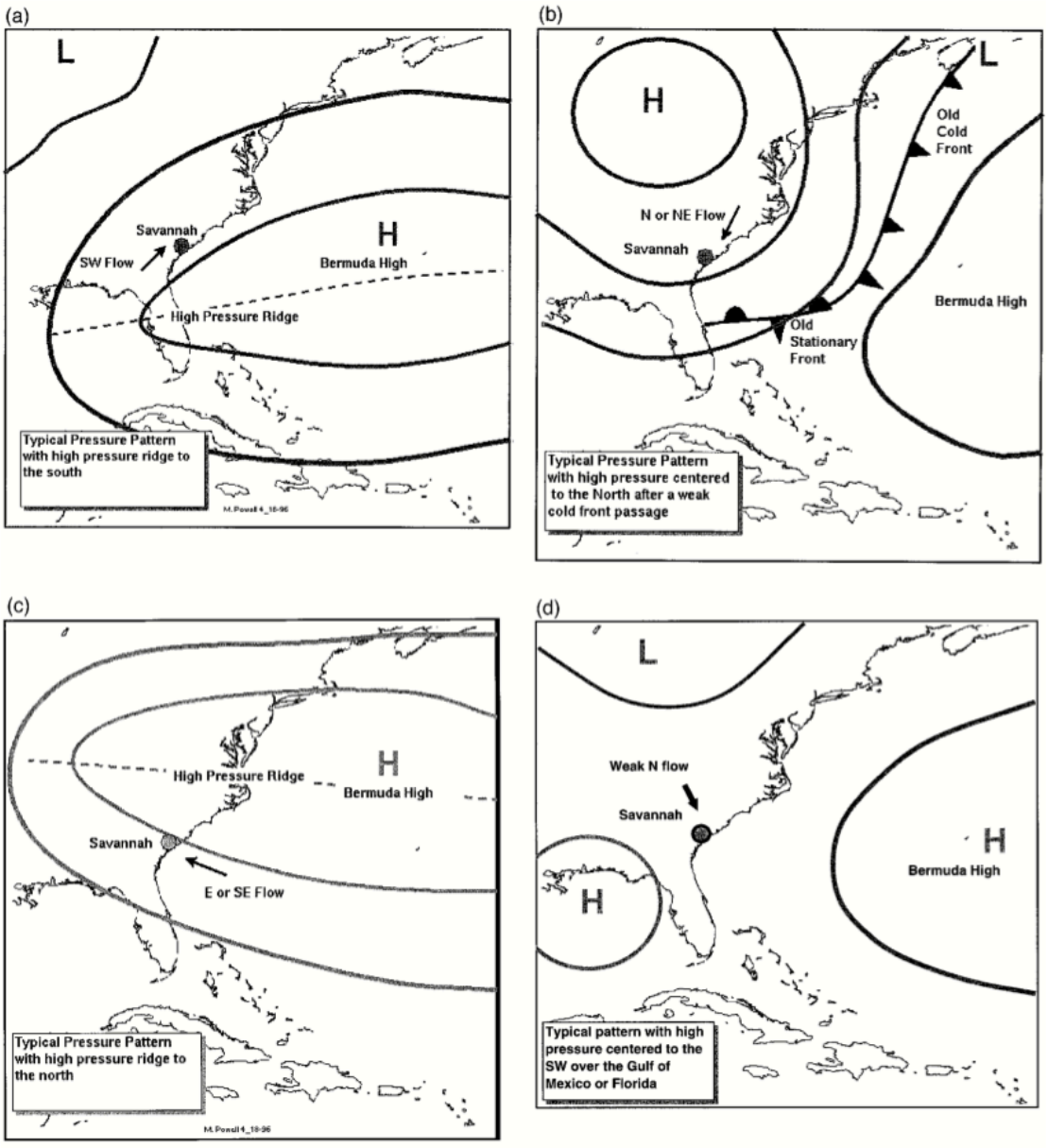

Fig. 1.2. Schematic from Powell and Rinard (1996). Panels show the surface synoptic features and the resultant gradient flow for non-disturbed synoptic days categorized by (a) high pressure ridge to the south, (b) high pressure centered inland to the north or northwest, (c) high pressure ridge to the north, and (d) high pressure centered to the southwest.

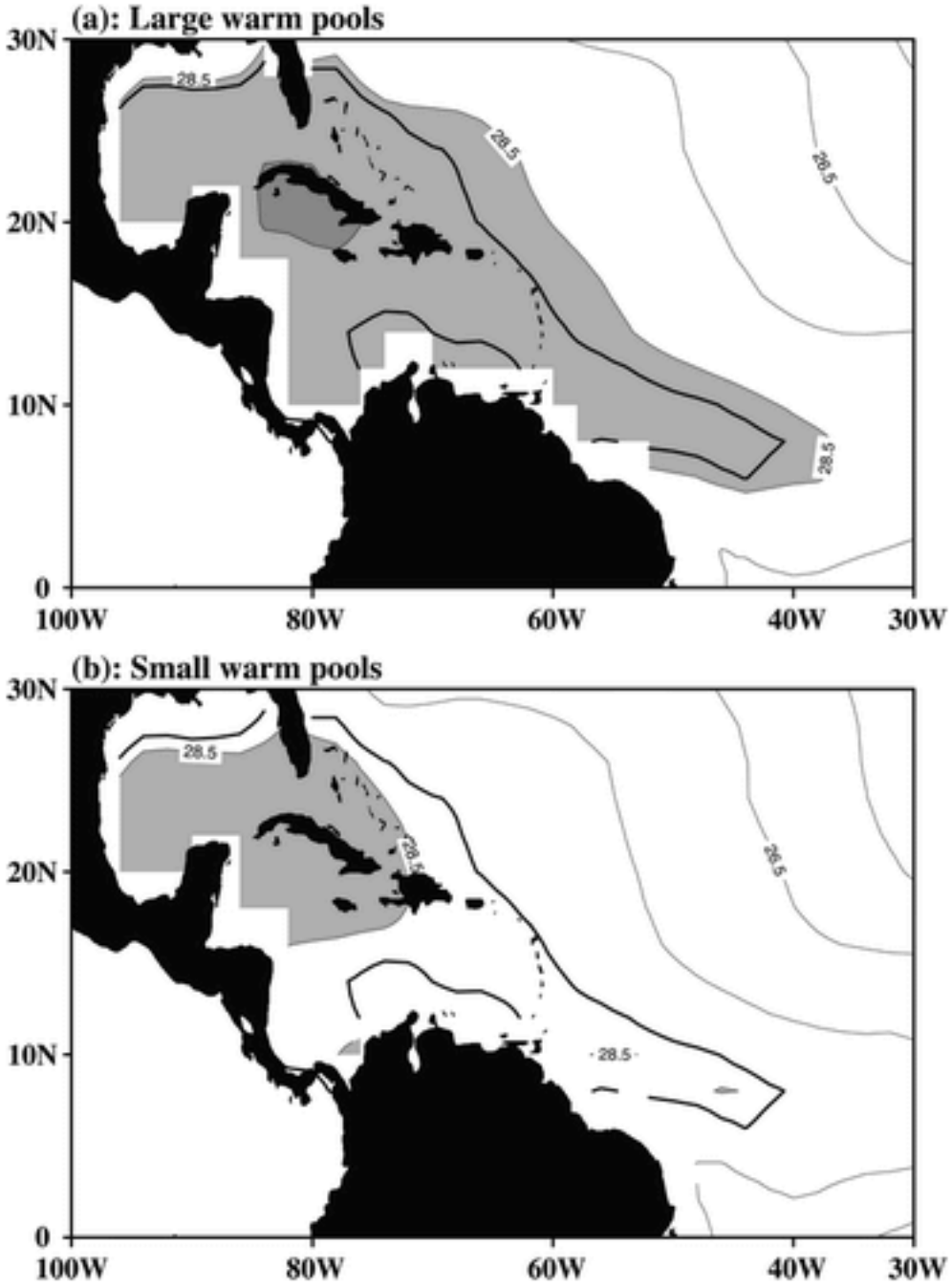

Fig. 1.3. Two schematics showing the AWP from Wang et al. (2006). Gray shading denotes the total area of SSTs greater than 28.5°C for (a) large AWP years and (b) small AWP years. The contours are isotherms in °C.

CHAPTER TWO

DATA AND METHODOLOGY

2.1 Datasets Used in Study

2.1.1 Model

This study uses the Center for Ocean-Atmospheric Prediction Studies (COAPS) Land Atmosphere Regional Reanalysis over the Southeast United States (CLARReS; Stefanova et al. 2011) to generate the majority of the atmospheric fields discussed in the results. CLARReS consists of the National Center for Environmental Prediction's (NCEP) Experimental Climate Prediction Center (ECPC) Regional Spectral Model (RSM; Juang and Kanamitsu 1994) with lateral boundary forcing from other reanalysis datasets. The RSM is a Fourier-based spectral model; its primitive equations are under the hydrostatic assumption. Table 2.1 shows a list of the parameterization schemes that are used, including the land cover dataset used and topographic information. A scale-selective bias corrective scheme (Kanamaru and Kanamitsu 2007) is also applied, which limits the large-scale errors often found in the interior domain of the regional model and allows the down-scaled fields to be less dependent on the domain.

The CLARReS model has two different versions, which are differentiated by the type of reanalysis dataset used as the boundary forcing. The first version was forced by the NCEP Department of Energy (DOE) Reanalysis II (R2; Kanamitsu 2002) dataset; the process of using global reanalysis as boundary forcing for regional models is known as dynamical downscaling. A general definition of downscaling is the process by which a coarse resolution atmospheric data set is brought to a finer resolution by integrating a higher resolution regional atmospheric model forced at the lateral boundaries by the coarse data set. The lateral boundary conditions was set by using wind, temperature, humidity, and surface pressure for every six hours from the R2. This version hereafter will be referenced as CLARReS1.0/R2. The other version is the same as the previous one except that instead of R2, the European Centre for Medium-Range Weather Forecasts (ECMWF) 40 Year Re-analysis (ERA-40; Uppala et al. 2005) was used. This integration of the model will hereafter be referenced as CLARReS1.0/ERA40. Lim et al. (2010) were successful with this downscaling process. In their study, the R2 reanalysis was downscaled to 20 km using the RSM. The precipitation fields were calculated by summing up the daily

precipitation each month, then averaging the monthly totals from 1990 to 2005. Lim et al. (2010) showed that the precipitation was in better agreement with the observations; the root mean square error of the monthly-averaged precipitation decreased by over 93% in comparison with the original R2 dataset.

The two model runs are integrated from 1979 to 2001, a 23-year period. The spatial domain of the CLARReS integrations consists of the area between 23.1°N and 37.5°N, and between 92.1°W and 75°W. This area covers almost the entire southeastern United States, the northeastern Gulf of Mexico, and parts of the extreme western Atlantic (Fig. 2.1). Since the study focuses on Florida, most of the total model domain is not presented.

The horizontal grid spacing on both model integrations is 10 km, which is considerably smaller than the 2.5° (~280 km) horizontal spacing that both the R2 and ERA-40 reanalysis contain. The native vertical resolution is 28 sigma terrain-following levels. After post-processing the model data is interpolated into 17 mandatory pressure levels; the vertical resolution decreases with height. The two-dimensional variables are available hourly, whereas the three-dimensional variables are only available every three hours, starting at 7:00 p.m. Therefore, results at three-hour intervals will be shown in the examination of the diurnal cycle. However, the two-dimensional fields are examined as well, and the results do not change because of the lower temporal spacing of the three-dimensional variables.

2.1.2 Verification and Other Datasets

Along with the two CLARReS model integrations (which are forced by observed SSTs), numerous other datasets are used. The SST used to force these model integrations is the extended reconstruction sea surface temperature version 3 (ERSSTv3; Smith et al. 2008), which is provided by the National Oceanic and Atmospheric Administration (NOAA). We also used R2 horizontal wind fields, which are monthly averaged and available on a 2.5°x2.5° grid. Both the ERSSTv3 and the R2 analyses have global spatial domains; therefore, they can be used to show the entire AWP.

Two different precipitation observational datasets are used to verify the model simulations of the diurnal and interannual variations. The first is the precipitation analysis from the Climate Prediction Center (CPC; Higgins et al. 2000), which consists of station data archives available at one-quarter degree resolutions. The domain for this dataset covers 140°W to 60°W and 20°N to 60°N, large enough to cover the contiguous 48 states. The smallest temporal spacing

that the CPC precipitation can achieve is daily, which makes it unsuitable for diurnal verification. Therefore, in conjunction with CPC, the NCEP Environmental Modeling Center (EMC) precipitation product (Lin and Mitchell 2005) produced by the National Weather Service (NWS) River Forecast Centers is used for verification. This product has 4-km grid spacing and is available hourly. NCEP-EMC precipitation is available only from 2002 to 2009, which, although it does not overlap with the CLARReS model temporal domain, is sufficient for verifying the climatological diurnal variability of precipitation.

2.2 Methodology

One of the first steps necessary for this study is to establish definitions of large and small AWP. To date, no categorization of the AWP has been accepted by the general scientific community because studies of the phenomenon are relatively recent (since 2001). Wang et al. (2006) adopted a definition based on their extended reconstructed SST dataset spanning the period from 1950 to 2003. Their study categorized large (small) AWP years as those in which the AWP size is 25% larger (smaller) than the climatological mean. Using this definition, they found that the large AWPs are almost three times larger than the small AWPs (Fig. 1.3).

The AWP size is calculated for the period 1979–2001 using the ERSSTv3 dataset, with the results shown in Fig. 2.2. For five of the years, AWP sizes are one standard deviation less than the mean (1984, 1986, 1989, 1993, 1994); for four of the years, AWP sizes are one standard deviation greater than the mean (1981, 1987, 1995, 1998). The remainder of the AWP sizes is between $3x10^6$ and $5x10^6$ m^2 with the exception of 1999, which has a slightly greater AWP size and is very close to the +1 standard deviation line. Therefore, 1999 is added to the large AWP composite; thus, each composite consists of five years. Table 2.2 shows the rankings of all the years.

Next, composites are made of SST and 850-hPa winds using this study's definition of large/small AWP (Fig. 2.3). These composites were computed using the summer months only (hereafter JJA) since the focus of this paper is sea breeze variations in Florida, which are most significant during JJA. Both the large and the small AWP composites are similar to the schematic provided by Wang et al. (2006; Fig. 1.3). Notice that even though most of the AWP is located in the Gulf of Mexico and the Caribbean Sea, the greatest changes take place in the Atlantic Ocean. Even so, the SSTs are generally warmer in the AWP during large AWP years. In conjunction with the SSTs, the 850-hPa winds also agree with the findings in Wang et al.

(2006) in that the background winds are weaker during large AWP years. These weaker flows are easily seen in the difference plot in the Gulf of Mexico and the Caribbean Sea (Fig. 2.3c). This figure is supported by the literature that describes a weakening of the Great Plains low-level jet (GPLLJ) during the large AWP case (Wang et al. 2006; Wang et al. 2008).

Climatological JJA precipitation composites are also created using the CPC observations (Fig. 2.4). The most striking difference between the large and small AWP years is the negative precipitation anomaly that exists in the Florida panhandle, especially west of 84˚W. Although this anomaly does not prove that the AWP modulates Florida convection, it does suggest the potential for low-frequency variations of the sea breeze to be present because of the AWP phenomenon. Although peninsular Florida, especially the interior, also shows a negative anomaly, the signal is weaker than in the panhandle, and thus less emphasis is placed on peninsular Florida. Therefore, cross sections appearing later will highlight the panhandle region between 84˚W and 88˚W to focus on the area that contains the strongest low-frequency signal.

The next section explores these low-frequency variations; a modulation is shown to exist; and the reason for the sea breeze variability for the Florida panhandle during JJA is diagnosed. These objectives are accomplished using a variety of spatial maps and cross sections. The cross sections are located along the latitude 30.5˚N since the emphasis will be on the Florida panhandle region (Fig. 2.5). This latitude is chosen to sample as much of the panhandle as possible and avoid the ocean as much as possible.

Table 1: A brief outline of the Regional Spectral Model.

Model Feature	**Description**
Grid Spacing	10-km horizontal grid spacing, 28 vertical terrain-following sigma levels
Domain	~ 23^0S to 37.5^0 N and 98^0W to 75^0W
Topography	30-min USGS topography
Vegetation map	USGS converted to 12 NOAH vegetation types (Loveland et al. 1995)
Land surface scheme	NOAH with 4 soil levels (Ek et al. 2003)
PBL scheme	Non-local; Hong and Pan (1996)
Radiation Scheme	Chou and Lee (1996); Chou and Suarez (1994)
Cloud water scheme	Diagnosed from relative humidity; Slingo (1987)
Convection scheme	Simplified Arakawa Schubert Scheme; Pan and Wu (1994)

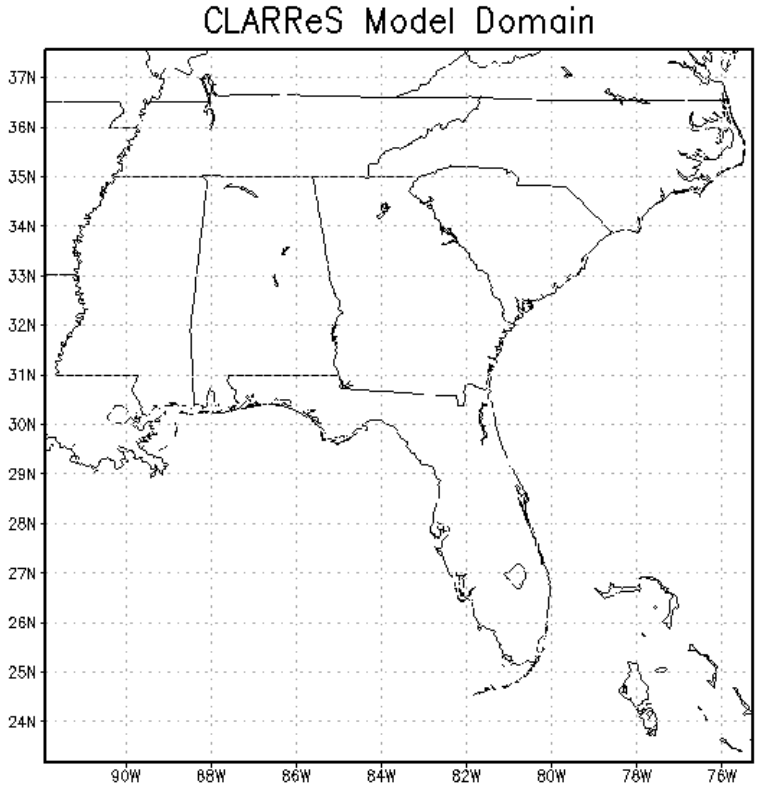

Fig. 2.1. The spatial domain of both the CLARReS1.0/R2 and CLARReS1.0/ERA40 model integrations.

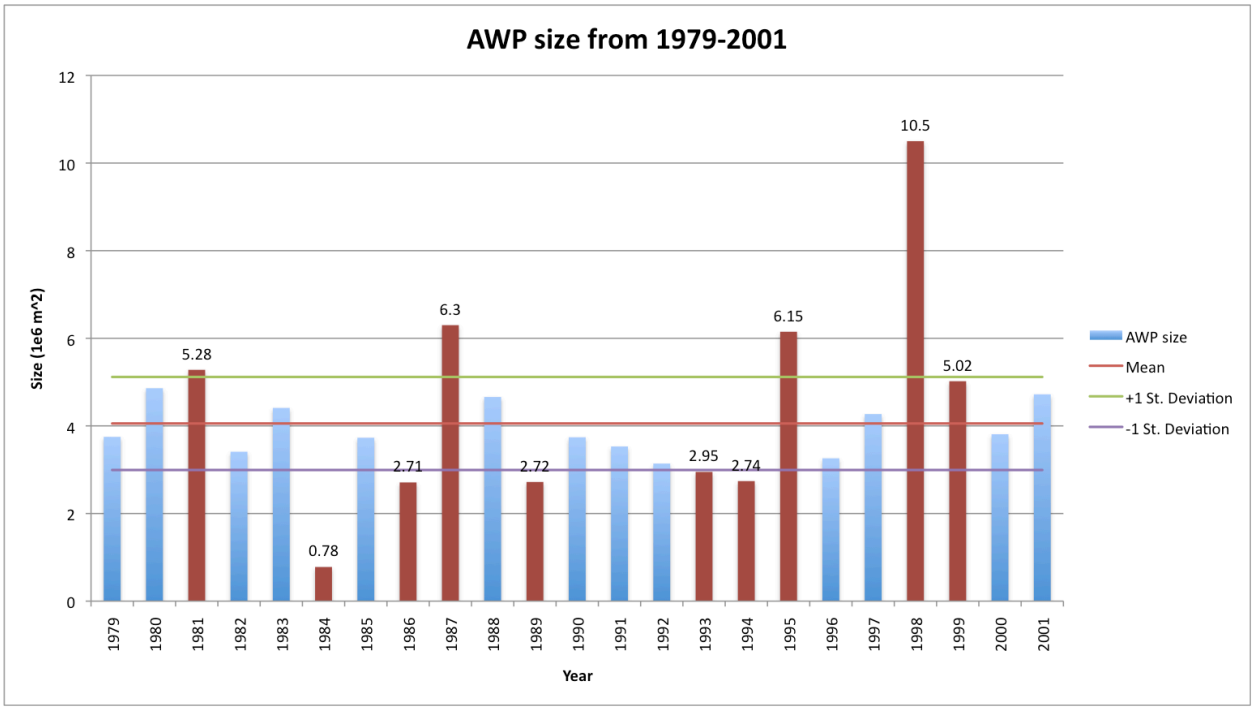

Fig. 2.2. Bar chart of AWP surface area. The year is on the x-axis, and the size (multiplied by $1x10^6$) is on the y-axis. The mean and the first standard deviation are shown (see legend to the right). The five greatest and five smallest sizes are denoted by red bars and labels.

Table 2: The year and the size of the AWP for that year. The years chosen to be large AWP years are in red, and the years chosen to be small AWP years are in blue. The years in black represent those that are designated as neutral AWP years.

Year	Size (10^6km)	Year	Size (10^6km)
1) 1998	1.05×10^7	13) 1990	3.74×10^6
2) 1987	6.30×10^6	14) 1985	3.73×10^6
3) 1995	6.15×10^6	15) 1991	3.53×10^6
4) 1981	5.28×10^6	16) 1982	3.41×10^6
5) 1999	5.02×10^6	17) 1996	3.26×10^6
6) 1980	4.86×10^6	18) 1992	3.14×10^6
7) 2001	4.72×10^6	19) 1993	2.95×10^6
8) 1988	4.66×10^6	20) 1994	2.74×10^6
9) 1983	4.41×10^6	21) 1989	2.72×10^6
10) 1997	4.27×10^6	22) 1986	2.71×10^6
11) 2000	3.81×10^6	23) 1984	7.82×10^5
12) 1979	3.75×10^6		

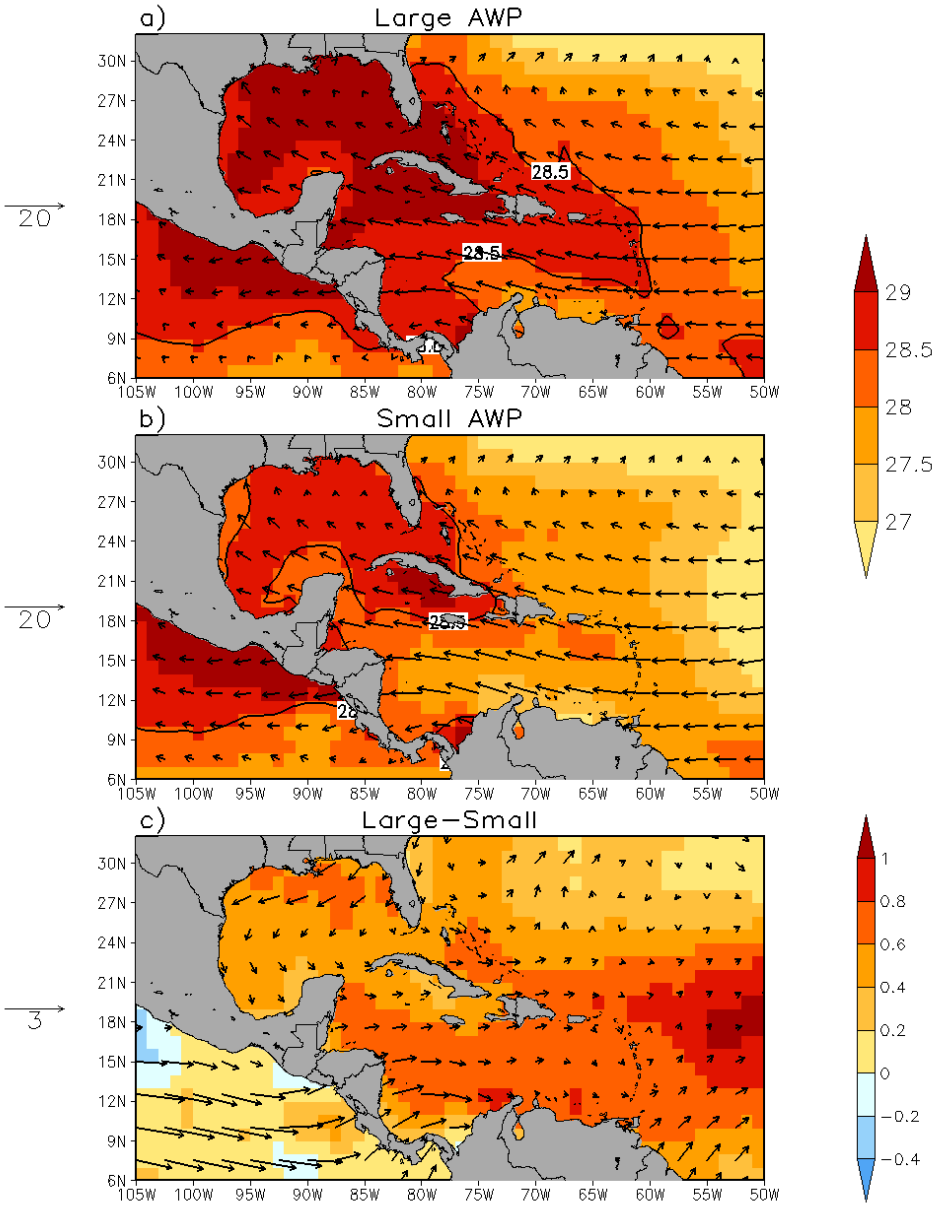

Fig. 2.3. The shading shows SST in units of ^{0}C from the ERSSTv3 observational dataset, and the vectors are 850-hPa winds taken from the NCEP-DOE R2 dataset (in units of m/s). The panels are (a) the large AWP summer (JJA) composite mean, (b) the small AWP JJA composite mean, and (c) the difference (large-small) between the two composite means. The scale vector is given by the arrow on the left of the panels.

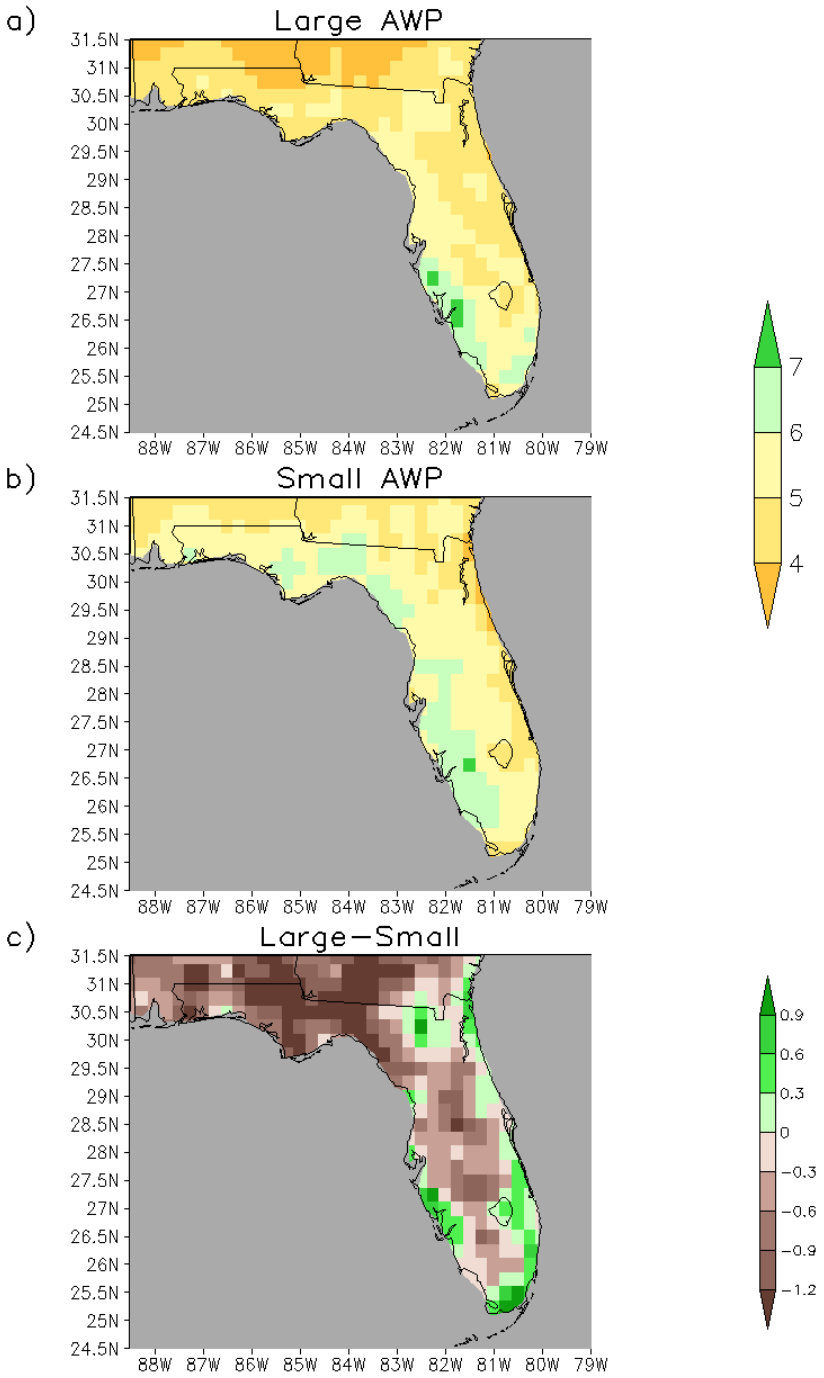

Fig. 2.4. Precipitation in units of mm day^{-1} for (a) the large AWP JJA composite mean, (b) the small AWP JJA composite mean, and (c) the difference (large-small) between the two composite means.

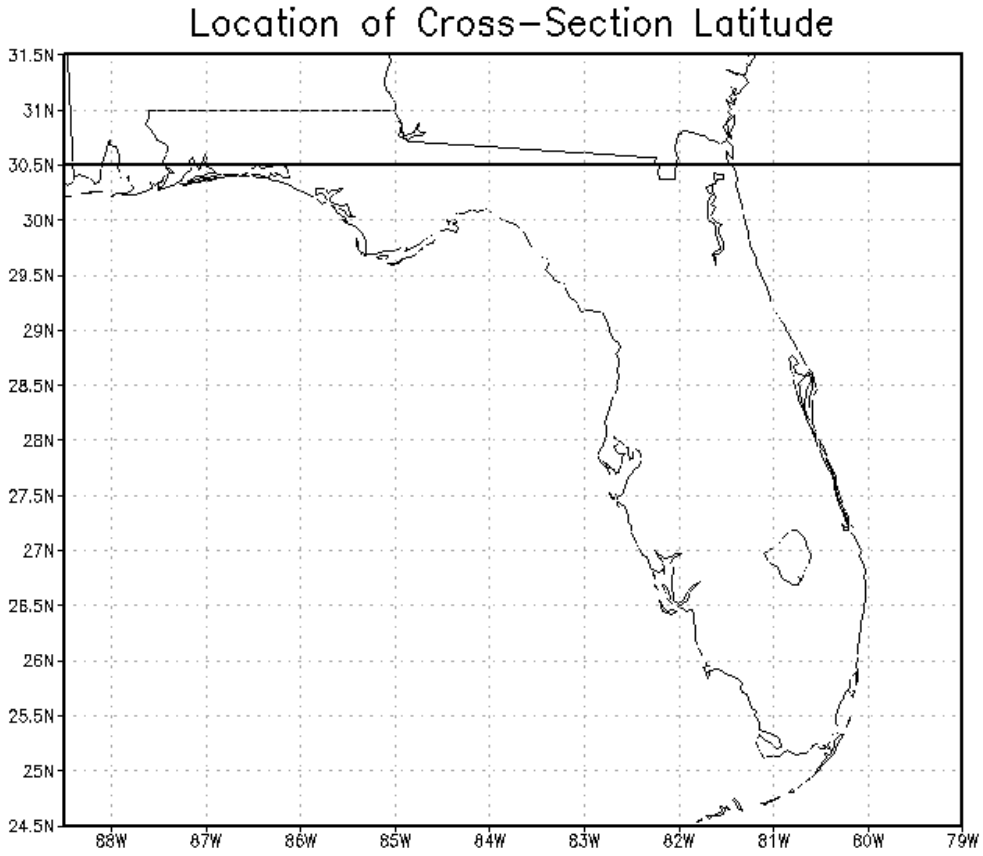

Fig. 2.5. The 30.5°N latitude and spatial domain for the majority of the area plots.

CHAPTER THREE

RESULTS

3.1 Climatology of the Diurnal Variability over Florida

This study first addresses the diurnal nature of the sea breeze and verifies the CLARReS model's ability to simulate diurnal changes in the sea breeze and associated convection. This objective is accomplished by first using the observations taken from the NCEP-EMC gridded precipitation estimates (Fig. 3.1) to examine the diurnal convection cycle. Figure 3.1 indicates that daily convection reaches a minimum at 4:00 a.m., with a gradual increase in precipitation occurring throughout the morning hours. Significant convection, most notably in southern Florida, arises at 1:00 p.m. The diurnal maximum of precipitation for the entirety of Florida occurs at 4:00 p.m., followed by a gradual decrease of precipitation into the overnight hours.

Figures 3.2 and 3.3 show the climatological mean diurnal precipitation cycle for CLARReS1.0/R2 and CLARReS1.0/ERA40, respectively. The smooth appearance of the contours in these models compared to the NCEP-EMC product is caused by the smaller grid spacing of the CLARReS model integrations. Both CLARReS1.0/R2 and CLARReS1.0/ERA40 underestimate the precipitation in comparison to the NCEP-EMC product; the extent of the underestimation changes throughout the diurnal cycle. Precipitation amounts exhibit a 40% difference throughout most of Florida during the afternoon. The precipitation maxima from both models are located in southern Florida and are slightly less than the NCEP-EMC maximum, all located in southern Florida. This observation of underestimation and maxima continue at 4:00 p.m. and 7:00 p.m., although the location of the precipitation maxima moves northward and inward as the evening commences. Overnight, the underestimation of the precipitation becomes minimal.

However, both model integrations capture the timing and nature of the diurnal cycle, which allows continuation of this study. CLARReS1.0/R2 and CLARReS1.0/ERA40 indicate precipitation minima occurring at 4:00 a.m. and precipitation maxima at 4:00 p.m. The growth and demise of the diurnal peak is also simulated well in both model integrations. The correct reproduction of the climatological average precipitation diurnal cycle was a primary motivation

for using the RSM downscaled models. Not only does it allow for study of the sea breeze in a systematic matter but downscaled models give gridded data of all atmospheric variables that are dynamically consistent.

In addition to precipitation, the climatological diurnal cycle of the planetary boundary layer (PBL) height and the vertical circulation (meridional and vertical winds) are plotted. These variables are averaged over a line of latitude (30.5°N; see Fig. 2.5 for a location reminder) using CLARReS1.0/R2 (Fig. 3.4) and CLARReS1.0/ERA40 (Fig. 3.5). Although many vectors point left and right, that is not a reference to west-east zonal movement. Rather, vectors pointing toward the right represent northerly flow and vectors pointing to the left indicate southerly flow. Using this reasoning, one can see that winds are from the south in the low levels over the panhandle; increased wind direction variability exists in the midlevels. Primary attention is focused west of 84°W where the panhandle coast meets the Gulf of Mexico.

Figure 3.4 shows that during the overnight hours the CLARReS1.0/R2 model has suppressed vertical motion over the Florida panhandle. Areas of slight vertical motion might correspond to the land breeze of the diurnal thermal circulation (Biggs and Graves 1962); the signal during the night is not as strong as during the day. The PBL is also quite shallow over land overnight, with increases occurring at 10:00 a.m., corresponding to the start of diurnal heating. The PBL reaches a maximum at 1:00 p.m., when the vertical velocities also increase. At 1:00 p.m., upward vertical velocities exist over the land areas that are near a coastline, and downward vertical velocities are beginning to show over water near land. The thermal circulation is noisier over the western part of the cross section, presumably an indirect result of numerous bays and other small water bodies in the area (Fig. 2.5). These vertical velocities reach a peak at 4:00 p.m. when the PBL height starts to decrease. Since the precipitation maximum is also at 4:00 p.m. the CLARReS1.0/R2 depicts this decreasing PBL because updrafts from the convection in the area have broken through the PBL and "mixed it out." The thermal circulation is unidentifiable by 7:00 p.m. and the PBL decreases to less than 500 m as night progresses. The large-scale flow becomes southerly in the low levels at this time. Therefore, the vertical circulation is showing diurnal variability with an identifiable peak (4:00 p.m.). While not exclusively, the sea breeze is also represented in the diurnal variability. The CLARReS1.0/ERA40 also demonstrates this diurnal picture with the main difference being stronger vertical velocities at 7:00 p.m.

3.2 Climatology of the Interannual Variability over Florida

The interannual variability of the precipitation is examined next. Figure 3.6 contains the AWP composites of CLARReS1.0/R2 precipitation and differences between the large and small AWP composites; the model's simulation of the interannual variability is evaluated by comparing it with the observations in Fig. 2.4. In the panhandle of Florida, CLARReS1.0/R2 overestimates the amount of precipitation for both composites by 20% to 30%. The locations of the precipitation maxima and minima also are not collocated. For example, the minimum in the observations during large AWP years is located in the northern parts of panhandle Florida reaching into Georgia and Alabama; the minimum in CLARReS1.0/R2 is featured along the southeast coast of the Florida peninsula. However, the model does appear to reproduce the precipitation maximums along the Gulf Coast of Florida during small AWP years. Another feature of note is that both composites correctly simulate the meridional gradient of precipitation from the Gulf coast to Alabama and Georgia. The interannual signal along peninsular Florida is not captured well in CLARReS1.0/R2, particularly across the region between Jacksonville and Tampa. There are several possible reasons for the model's inability to capture the interannual signal. One is the complicated nature of sea breeze interactions in this part of the state caused by interactions of the east coast and west coast sea breeze. Another is that the peninsula of Florida experiences more tropical cyclones than its panhandle counterpart, which introduces a component unrelated to the diurnal precipitation and thermal circulation. What the model does simulate well is the strong negative anomaly along the panhandle of Florida west of 84˚W as well as highlight that precipitation does vary between large and small AWP years.

CLARReS1.0/ERA40 (Fig. 3.7) does worse than CLARReS1.0/R2 (Fig. 3.6) in simulating the precipitation, showing overestimation over most of the region in both composites. This model integration persistently shows high precipitation maxima in South Florida, unlike CLARReS1.0/R2 and the observations. CLARReS1.0/ERA40 has difficulty simulating the interannual variability of the precipitation in peninsular Florida because of the inherently more complicated nature of the sea breeze in this region. The composite difference for CLARReS1.0/ERA40 is similar to CLARReS1.0/R2, except that the positive precipitation anomalies are more pronounced over central Florida, and the negative anomalies are farther west (86˚W-88˚W) in the panhandle.

Both model integrations show agreement in the negative anomaly for large AWP years over the panhandle of Florida. The rest of the chapter will focus on explaining the low-frequency variations of the sea breeze and related convection over the Florida panhandle, primarily west of 84°W. At this point closer study of peninsular Florida will be discontinued because the low-frequency variations of the sea breeze in that region are not distinguishable. CLARReS1.0 has difficulty simulating this region due to the more complicated nature of the mesoscale and synoptic systems in peninsular Florida.

3.3 Diagnostic Analysis of the Low-frequency Variations over Panhandle Florida

The first step in identifying the mechanism behind the interannual variability is to examine the temperature gradient between the land and sea because the differential heating between them produces the sea breeze. Both CLARReS1.0/R2 (Fig. 3.8) and CLARReS1.0/ERA40 (Fig. 3.9) exhibit good agreement with the composite mean temperatures. During large AWP years the land temperatures are slightly warmer than during small AWP years. Ocean temperatures are relatively constant compared to the land temperature changes due to the higher heat capacity of water; they do not change significantly on a day-to-day basis. Therefore, the increased heating over land for large AWP years by both model integrations suggests that the temperature gradient between land and ocean is greater during large AWP years. A stronger temperature gradient increases the strength of the thermal circulations, enhances the sea breeze, and thus leads to more convection. Thus, there is a contradiction between sea breeze strength and precipitation during large AWP years since a larger temperature gradient is present but less convection falls over the Florida panhandle.

The diurnal change of the composite differences of precipitation is examined next. The CLARReS1.0/R2's precipitation is shown in Fig. 3.10, and the CLARReS1.0/ERA40's precipitation is shown in Fig. 3.11. CLARReS1.0/R2 shows a rainfall deficit during large AWP years compared to small AWP years in the Florida panhandle that are strongest at 4:00 p.m., and the precipitation pattern at 4:00 p.m. matches the seasonal composite difference (Fig. 3.6c). This match suggests that the sea breeze and precipitation are modulated by interannual variations of the AWP. Figure 3.11 does not show the negative precipitation anomaly over the panhandle of Florida, but because of the westward displacement (Fig. 3.7c) of the negative anomaly, it is more difficult to complete this analysis for the CLARReS1.0/ERA40 integration. However, the precipitation patterns at 1:00 p.m. and 4:00 p.m. closely match the seasonal composite mean

difference (Fig. 3.7c), and negative anomalies are present west of 86°W. Even though the signal is not as strong as that in CLARReS1.0/R2, CLARReS1.0/ERA40 also supports modulation of the sea breeze and convection by the AWP variations.

The interannual modulation of the sea breeze seems apparent; however, the evidence provided to explain the low-frequency variations in the sea breeze convection is contradictory to the observed interannual changes in the air/sea temperature gradient. Therefore, the large-scale effects on the interannual variability are examined. The idea that the large-scale flow influences the sea breeze is well supported in the literature (see Chapter 1). The cross section of the PBL and meridional and vertical winds is revisited; however, this time the composite mean difference at 4:00 p.m. is plotted for CLARReS1.0/R2 (Fig. 3.12) and CLARReS1.0/ERA40 (Fig. 3.13). The increased PBL depth during large AWP years is expected for two reasons. If there is less or weaker convection, the updrafts will not push through the inversion and disrupt the PBL as much, and if the land temperatures are warmer, more convectively-driven turbulence is generated, increasing the depth of the PBL. The thermal circulations are apparent at this time during both the large and small AWP years, and they seem to be more pronounced for the large AWP years (Figs. 3.12a, 3.13a). Another feature of note (Figs. 3.12c and 3.13c) is that anomalously large-scale subsidence takes place during large AWP years (although it is displaced westward in CLARReS1.0/ERA40).

One explanation of the large-scale subsidence anomaly is that it is related to the North Atlantic subtropical high (NASH, Fig. 3.14). Preliminary work by Li et al. (2011) showed that large-scale subsidence over the Southeast is related to the NASH. Wang et al. (2006) also described changes in NASH that were related to the variability of the AWP. Figures 3.15 and 3.16 show the composite mean and difference of mean sea level pressure and 850-mb winds from CLARReS1.0/R2 and CLARReS1.0/ERA40, respectively. Both model integrations show that during large AWP years, the NASH weakens and is displaced farther eastward. The NASH variations, in turn, introduce an anomalous meridional flow towards the equator over the southeast United States and the Florida panhandle (Figs. 3.15c, 3.16c). Thus, the anomalous meridional flow and large-scale subsidence are collocated over the Florida panhandle. These components are related based on the principles of Sverdrup vorticity balance (Rodwell and Hoskins 2001).

Hoskins (1996) described interactions between monsoon heating and the persistence of subtropical anticyclones using Sverdrup vorticity balance (Fig. 3.17). As the summer begins, the monsoon heating over land moves poleward. The movement of the monsoon forces the descent to intensify westward and poleward of the monsoon heating over the ocean. Over the ocean, the air aloft is relatively dryer than near the surface. The descent of dryer air into a layer will cause a decrease in cloud cover, and more outgoing long-wave radiation will escape the layer. Thus, the descent causes enhanced diabatic cooling (caused by radiative processes) that in turn enhances the descent, generating a positive feedback loop. Then, to maintain Sverdrup vorticity balance, equatorward flow occurs over regions of maximum descent. Sverdrup vorticity balance describes a relationship between the meridional flow and vertical motion (Rodwell and Hoskins 2001, Zhou et al. 2009).

The derivation the Sverdrup vorticity balance starts with the absolute vorticity equation,

$$\frac{d(\zeta + f)}{dt} = -(\zeta + f)\vec{\nabla}\cdot\vec{V} + Twisting + Solenoidal \qquad (1)$$

where ζ is the relative vertical vorticity and f is the Coriolis parameter. To obtain Sverdrup vorticity balance, assumptions are applied to the above equation. The first assumption is that for large-scale flow the last two terms can be neglected; when applying this assumption the vertical advection is also assumed to be negligible. Applying these assumptions and expanding the total derivative in (1) leaves

$$\frac{\partial(\zeta + f)}{\partial t} + u\frac{\partial(\zeta + f)}{\partial x} + v\frac{\partial(\zeta + f)}{\partial y} = -(\zeta + f)\vec{\nabla}\cdot\vec{V} \qquad (2)$$

The tropics and subtropics are not prone to small-scale weather-related phenomena. The variability of relative vorticity is negligible under these conditions, and thus the Coriolis term is dominant.

$$\frac{\partial f}{\partial t} + u\frac{\partial f}{\partial x} + v\frac{\partial f}{\partial y} = -f(\vec{\nabla}\cdot\vec{V}) \qquad (3)$$

The second term on the left-hand side can be neglected because the Coriolis force does not vary along latitude. The last assumption is to assume a steady state.

$$v\frac{\partial f}{\partial y} = -f(\vec{\nabla}\cdot\vec{V}) \qquad (4)$$

Equation (4) describes the Sverdrup vorticity balance. If one applies the continuity equation, the relation takes a form that is most common in the literature.

$$\frac{\partial f}{\partial y} = \beta$$

$$\frac{\partial u}{\partial x} + \frac{\partial v}{\partial y} = \vec{\nabla} \cdot \vec{V} = -\frac{\partial \omega}{\partial p}$$

$$\beta v = f \frac{\partial \omega}{\partial p} \qquad (5)$$

Both (4) and (5) show how the Sverdrup relationship works. When there is poleward flow, rising motion exists; for equatorward flow, sinking motion exists.

To examine the left-side term, the meridional flow from both model integrations (Figs. 3.18, 3.19) is plotted along the 30.5°N latitude. The composite differences show that both CLARReS1.0/R2 and CLARReS1.0/ERA40 indicate anomalous equatorward flow during large AWP years. Then, to complete the investigation of the equation, omega from both model integrations is shown in Fig. 3.20 (CLARReS1.0/R2) and Fig. 3.21 (CLARReS1.0/ERA40). Positive omega in regions west of 84°W in Fig. 3.20 shows that there is large-scale subsidence. The CLARReS1.0/ERA40 simulates the same process, although it displaces the subsidence westward by 2° longitude. This displacement is expected given the location of the subsidence and precipitation anomalies previously noted (Figs. 3.13, 3.7). Therefore, both of the model integrations indicate the Sverdrup vorticity balance as the mechanism that links the large-scale flow pattern to areas of descent. The main driver of this mechanism is the position and intensity changes of the NASH.

From Sverdrup vorticity balance, it follows that during large AWP years the NASH forces subsidence over the panhandle of Florida, which is not conducive to the development of precipitation even with a stronger land-sea temperature contrast. We now proceed further to examine the moisture budget of the sea breeze. The moisture balance equation used is:

$$\underset{Term1}{\frac{\partial Q}{\partial t}} = \underset{Term2}{-\nabla \cdot M} + \underset{Term3}{E} - \underset{Term4}{P}, \qquad (6)$$

where

$$-Q = \frac{1}{g} \int_{p_s}^{10mb} q dp$$

and

$$M = \frac{1}{g} \int_{p_s}^{10mb} \vec{V} q dp$$

In (6), term 1 is the precipitable water tendency term; term 2 is the moisture flux convergence term (where positive values indicate convergence); term 3 is evaporation; term 4 is precipitation. The terms of the moisture budget equation are plotted for both model integrations (Figs. 3.22, 3.23) at 4:00 p.m., where the precipitable water tendency term is calculated as a residual. CLARReS1.0/R2 and CLARReS1.0/ERA40 produce good agreements in the various terms.

The composite differences reveal anomalous convergence of moisture flux over the panhandle of Florida, especially in regions west of 84°W. The reasons for this anomaly were not investigated, but it is possible that the anomaly is due to stronger circulations occurring during large AWP years (Figs. 3.12, 3.13). The precipitation fields were discussed at length earlier (Figs. 3.10 and 3.11). Both models illustrate that evaporation is not significant factor in producing the interannual variability and thus can be discarded. The precipitable water tendency residuals should be strongly positive, as Figs. 3.22d and 3.23d indicate. The anomalous precipitable water is shown in Figs. 3.24 and 3.25. The composite difference in both model integrations shows that the precipitable water content is greater at 4:00 p.m. during large AWP years. Therefore, the precipitable water in the atmospheric column is anomalously positive during large AWP years, consistent with previous figures (Figs 3.22 and 3.23).

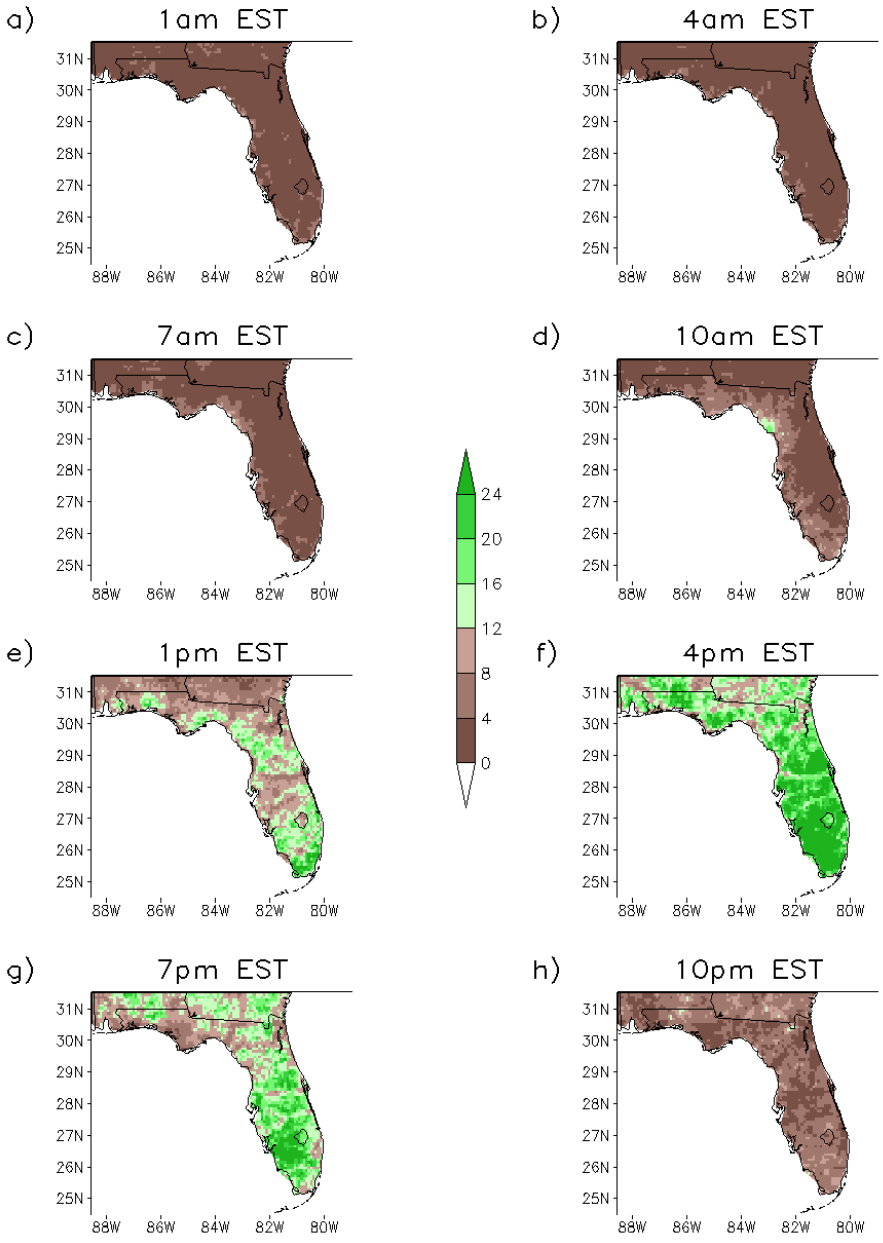

Fig. 3.1. Plot containing precipitation averaged at one time (denoted by the panel titles) over JJA for the entire temporal domain (1979-2001). The units are in mm day^{-1}. Precipitation data are from the NCEP-EMC dataset.

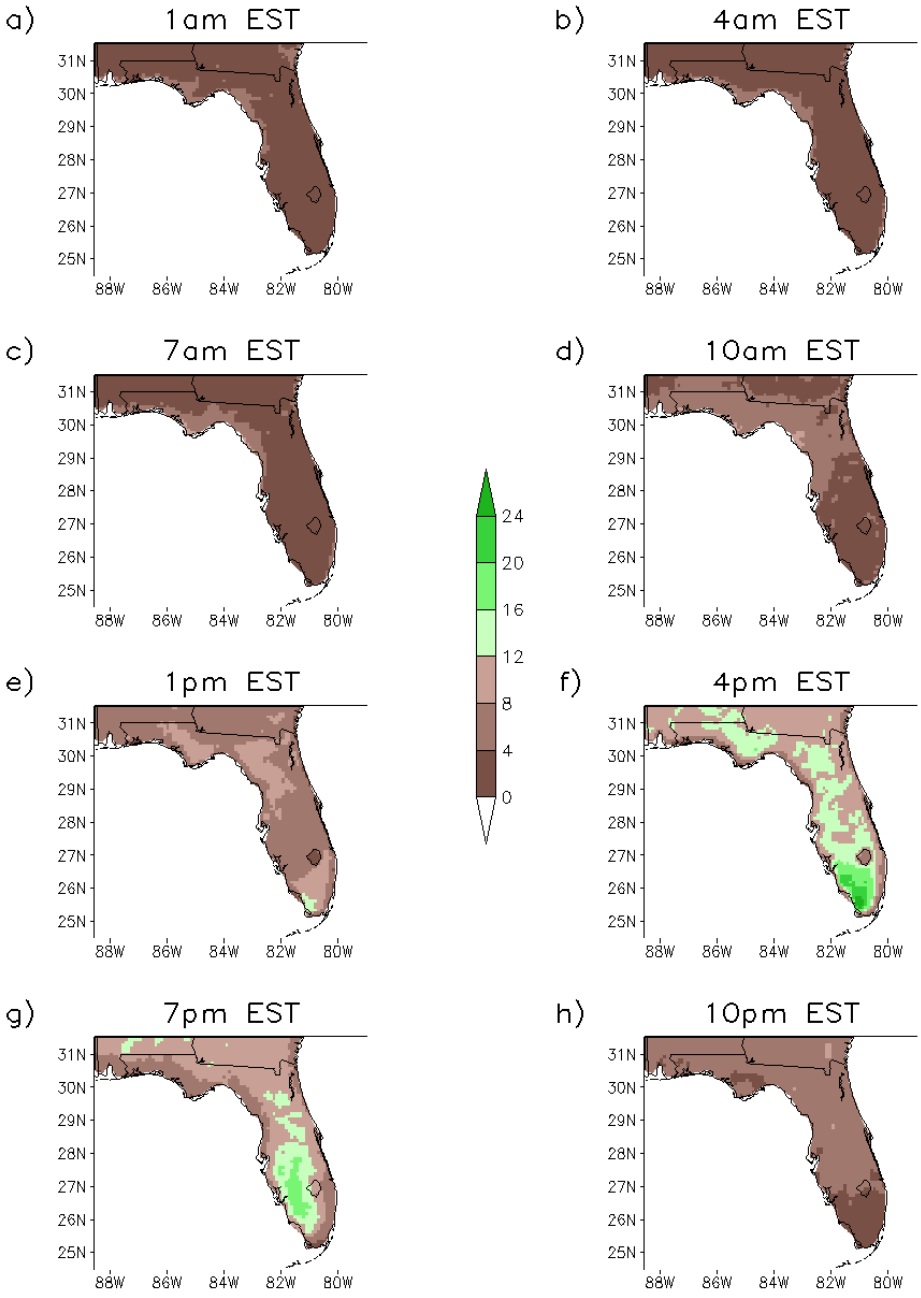

Fig. 3.2. Same as Fig. 3.1 except the data are from the CLARReS1.0/R2 model run.

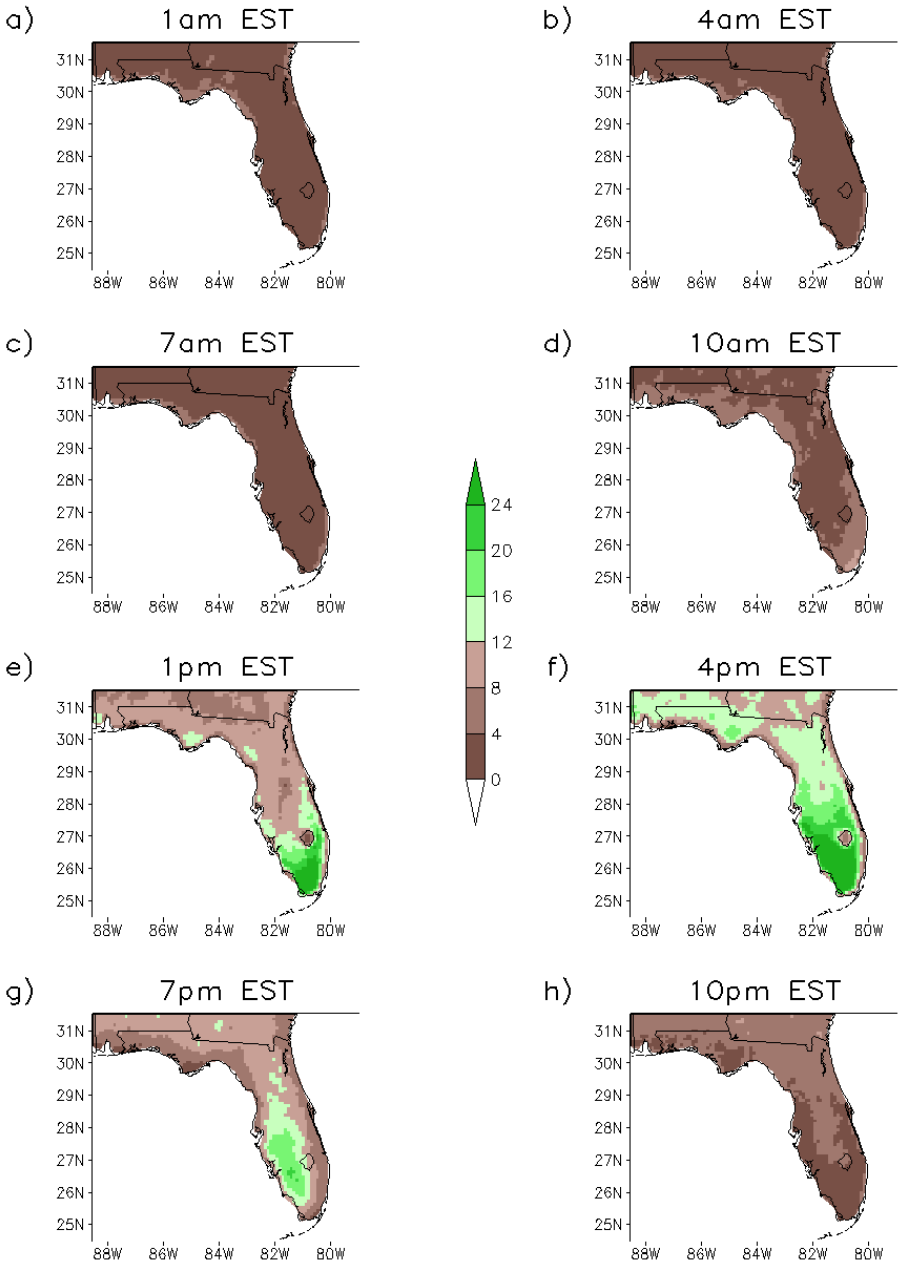

Fig. 3.3. Same as Fig. 3.1 except the data are from the CLARReS1.0/ERA40 model run.

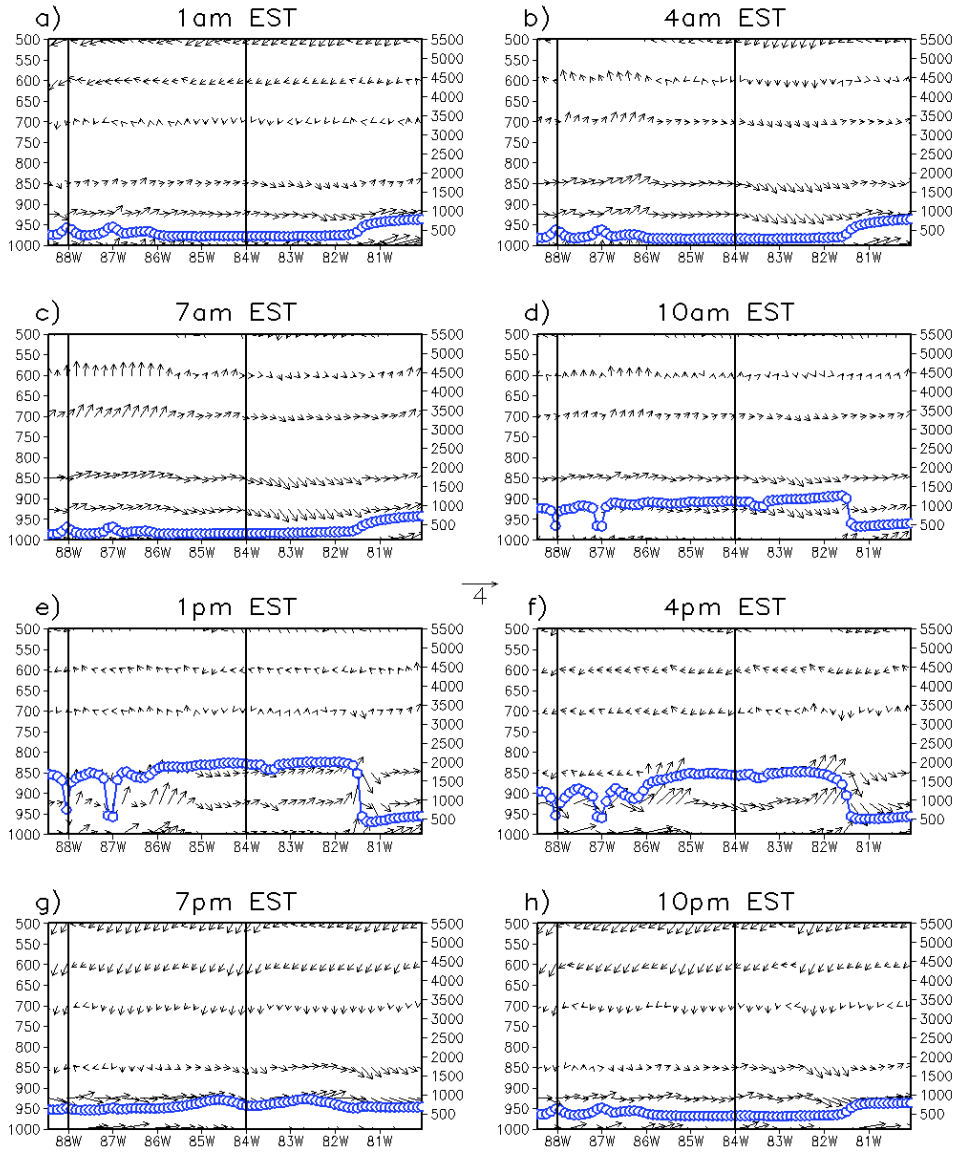

Fig. 3.4. Cross sections through 30.5˚N. The vectors indicate the meridional and vertical wind components from the CLARReS1.0/R2 model integration averaged at one time (denoted by the panel titles) over JJA from 1979 to 2001 in units of m/s. The vertical velocities are scaled by 100, and the arrow in the middle gives the scale vector. The left y-axis denotes height in hPa as a reference to the wind. The blue contour is the planetary boundary layer height in meters from the CLARReS1.0/R2 model integration, averaged the same way as the winds. Values are along the right y-axis. The black perpendicular lines mark the locations of 84˚W and 88˚W.

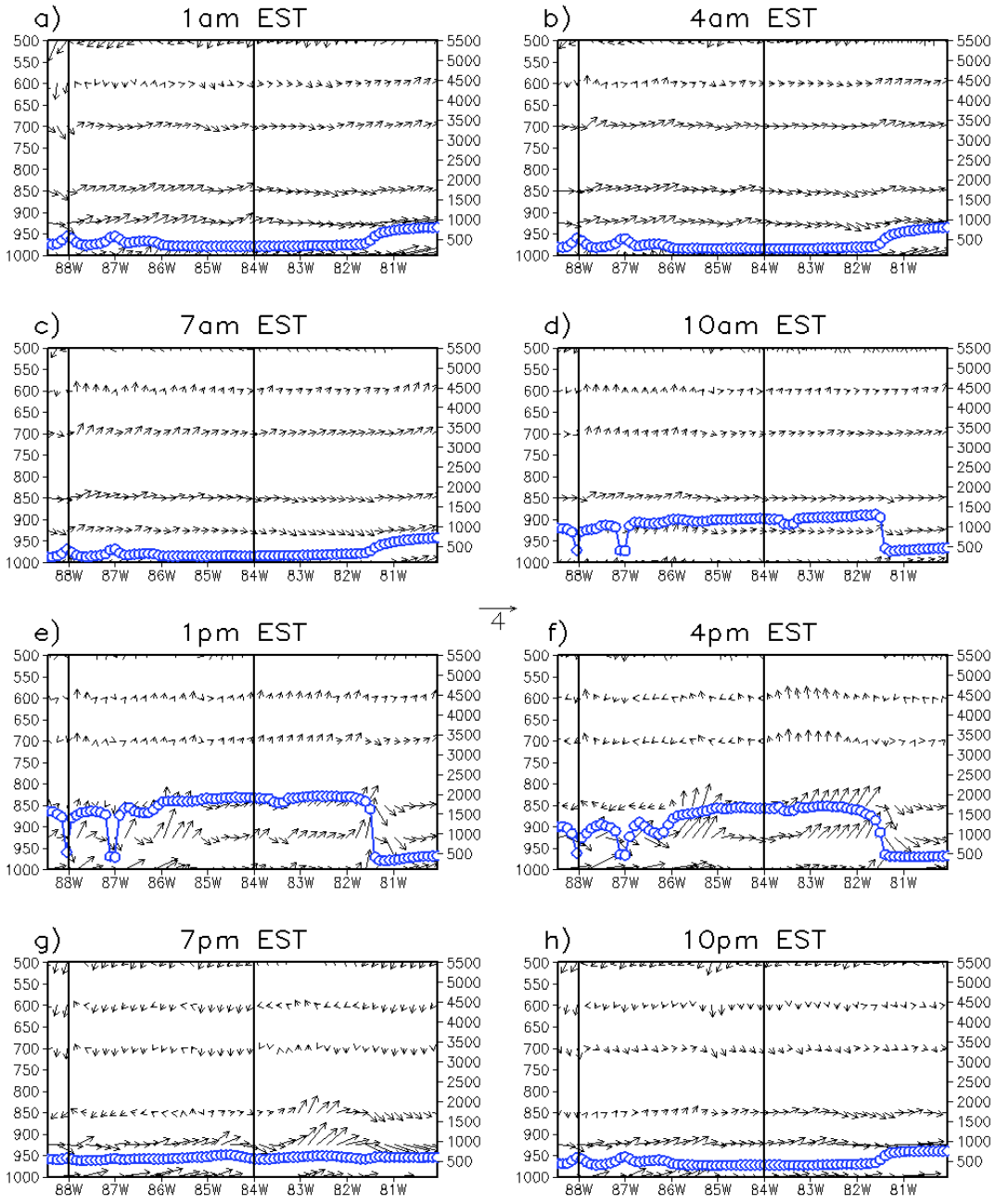

Fig. 3.5. Same as Fig. 3.4 except the variables are from the CLARReS1.0/ERA40 model run.

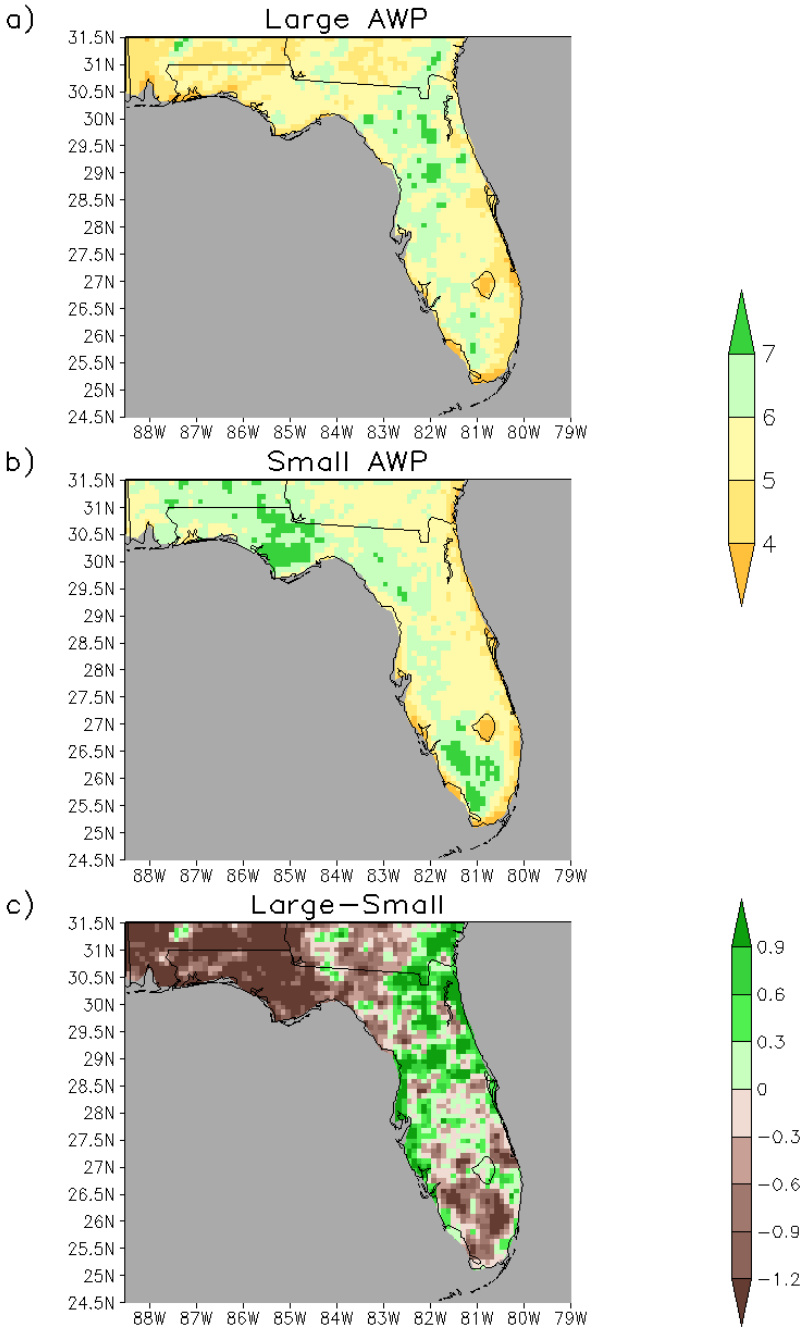

Fig. 3.6. Same as Fig. 2.4 except the data are from the CLARReS1.0/R2 model run.

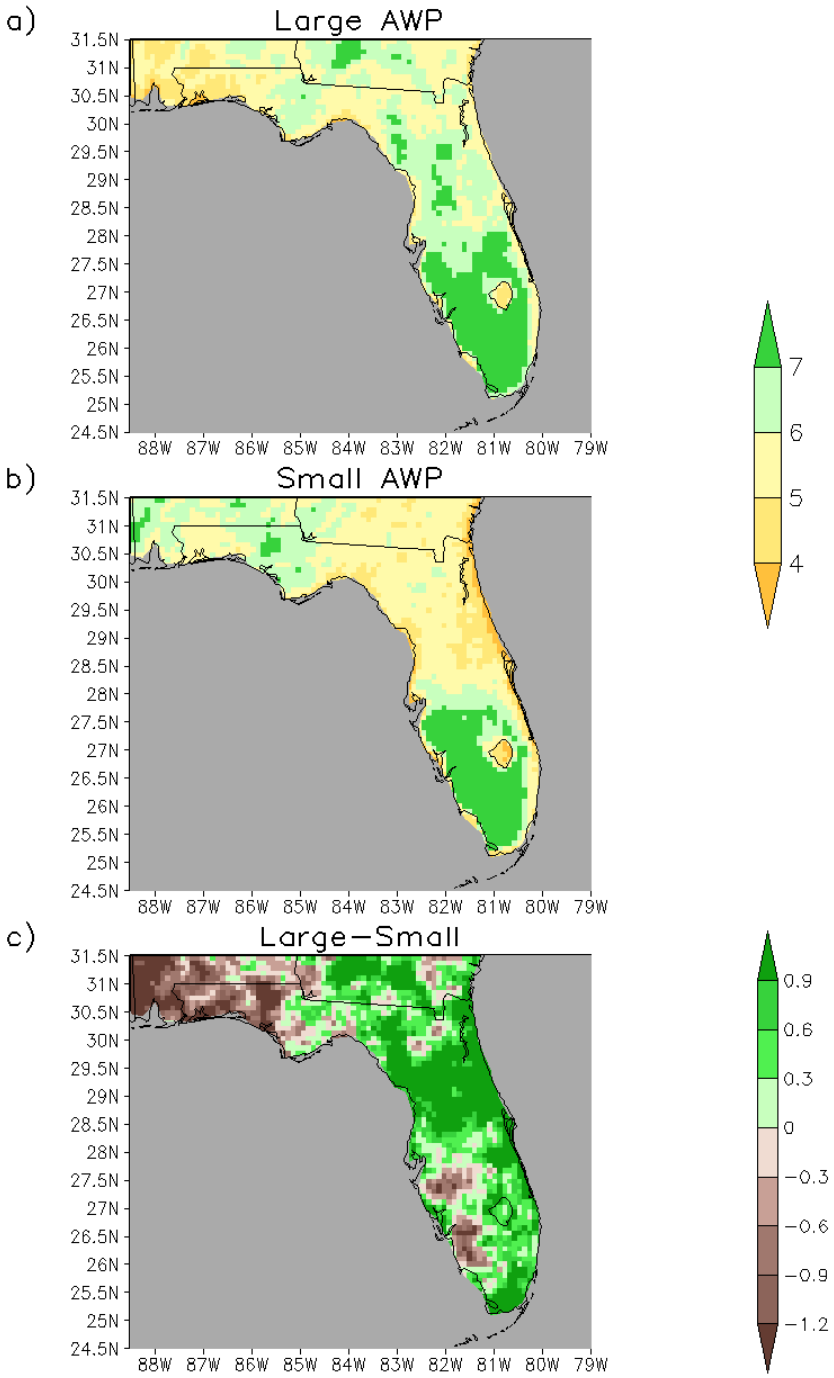

Fig. 3.7. Same as Fig. 2.4 except the data are from the CLARReS1.0/ERA40 model run.

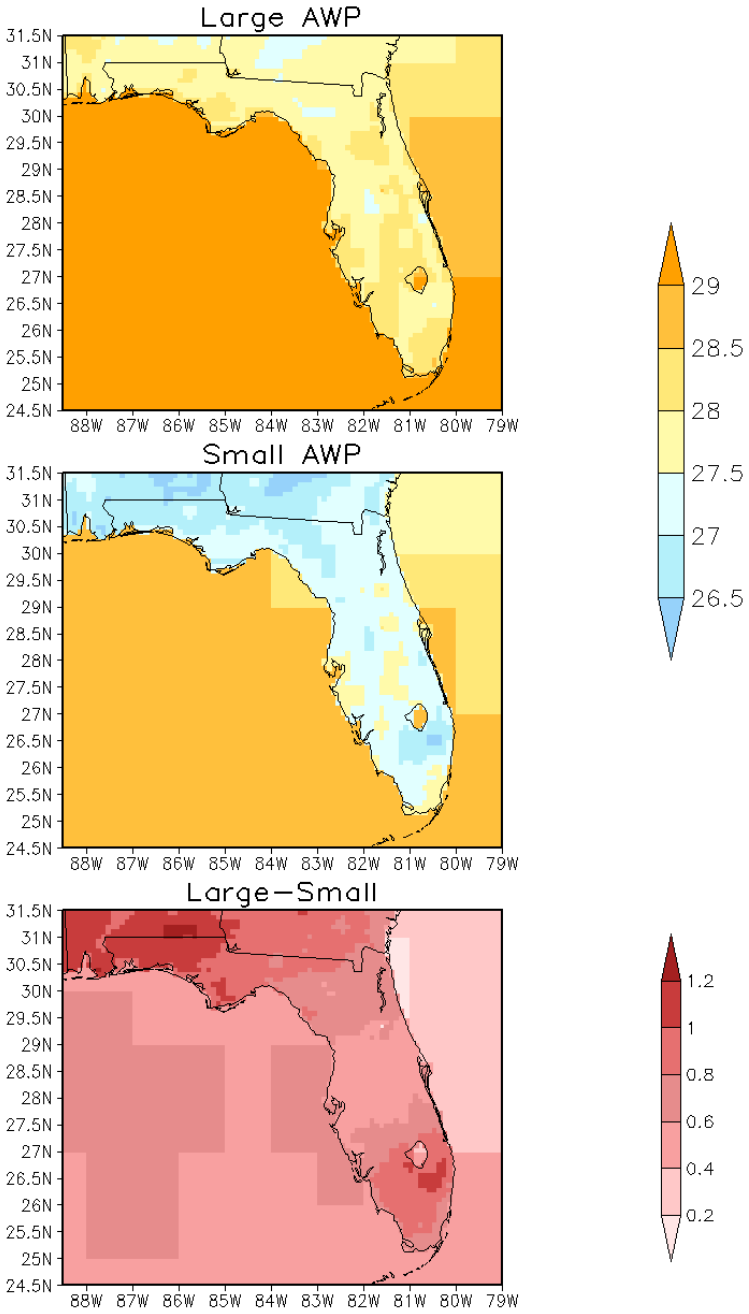

Fig. 3.8. AWP temperature composites. Over land, the shading denotes temperatures from the CLARReS1.0/R2 model integration in units of ˚C. Over the ocean/Gulf of Mexico the shading shows the SST in units of ^{0}C from the ERSSTv3 observational dataset. The panels are (a) the large AWP summer (JJA) composite mean, (b) the small AWP JJA composite mean and (c) the difference (large-small) between the two composite means.

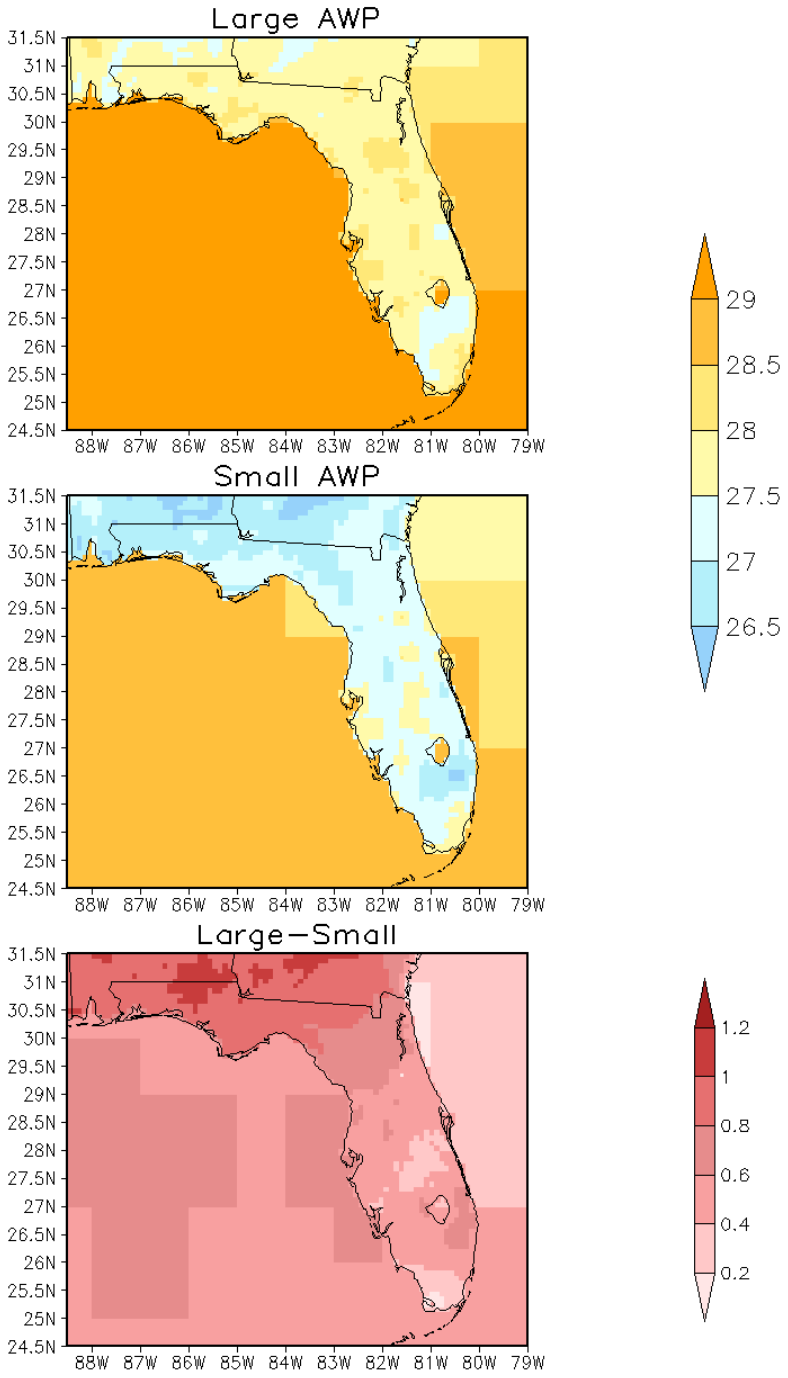

Fig. 3.9. Same as Fig. 3.8 except the data are from the CLARReS1.0/ERA40 model run.

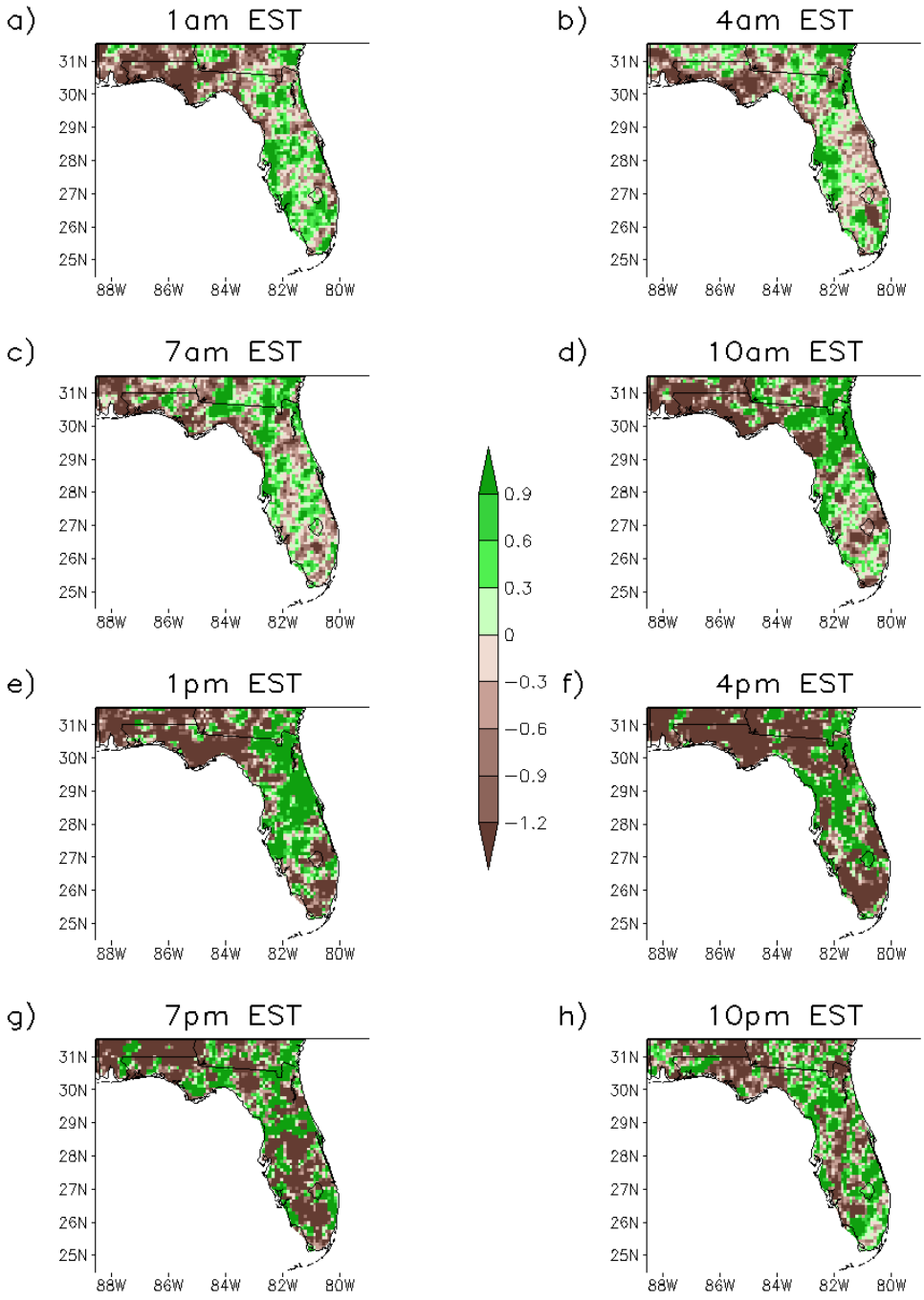

Fig. 3.10. Composite mean differences of precipitation in units of mm day^{-1} from the CLARReS1.0/R2 model run. These composites were averaged at one time (denoted by the panel titles) over JJA from 1979 to 2001 for large and small AWP years, and then the composites were subtracted from each other to obtain the composite mean difference.

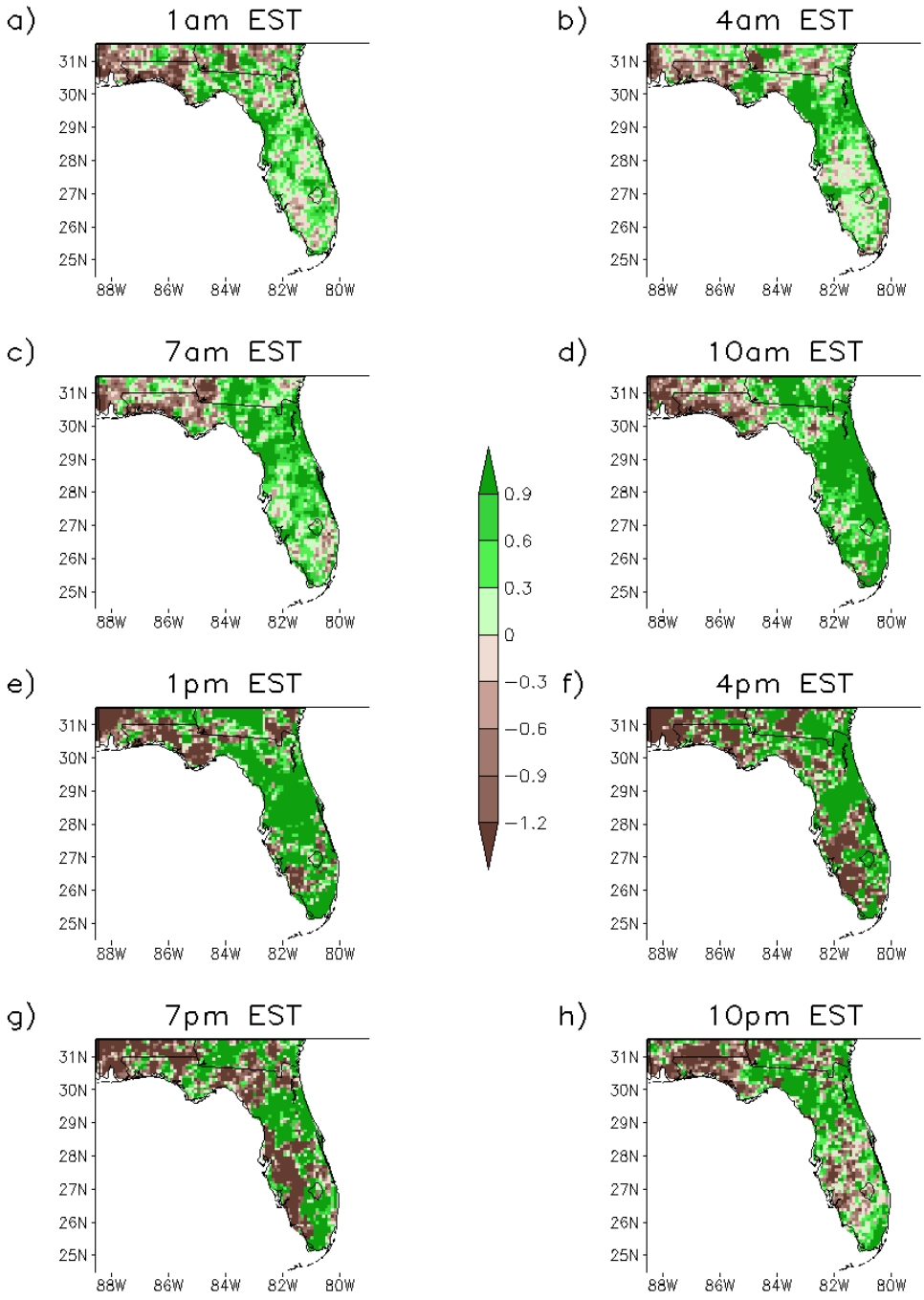

Fig. 3.11. Same as Fig. 3.10 except the data are from the CLARReS1.0/ERA40 model run.

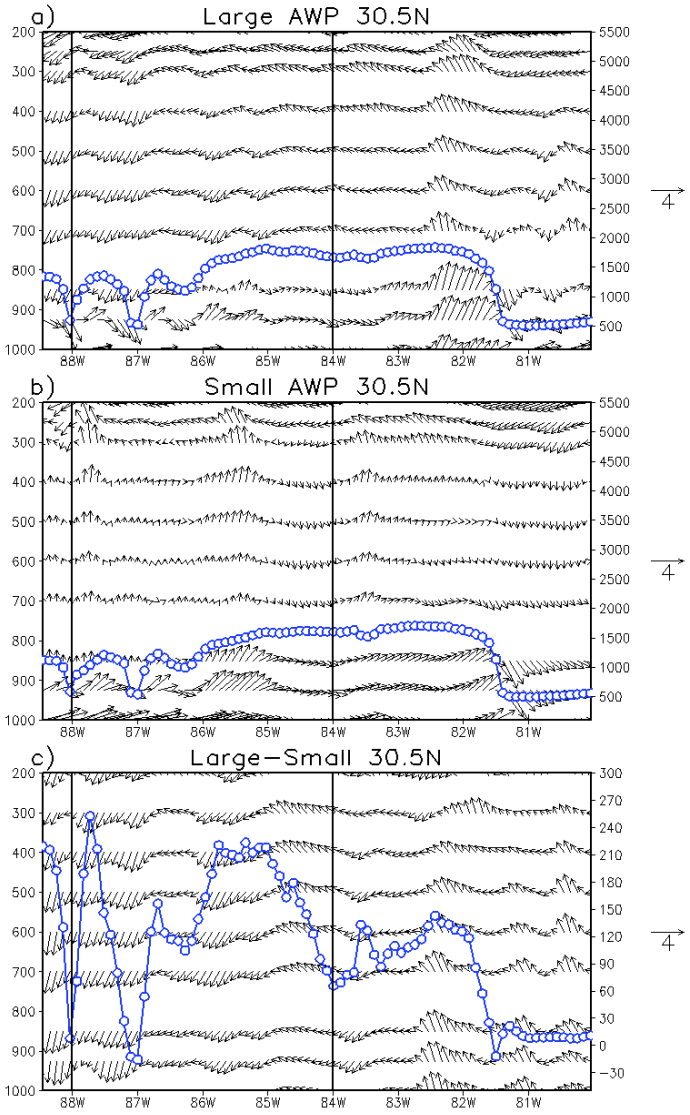

Fig. 3.12. Cross sections through 30.5°N. The vectors indicate the meridional and vertical wind components in units of m/s taken from the CLARReS1.0/R2 model integration, in which the vertical velocities are scaled by 100. The arrow to the right of each plot gives the vector scale. The left y-axis denotes the height in hPa. The blue contour is the planetary boundary layer height from the CLARReS1.0/R2 model integration in meters, which are along the right y-axis. The panels are (a) the large AWP climatological mean composite at 4:00 p.m., (b) the small AWP climatological mean composite at 4:00 p.m. and (c) the difference (large-small) between the 4:00 p.m. composites. The black perpendicular lines mark the locations of 84°W and 88°W.

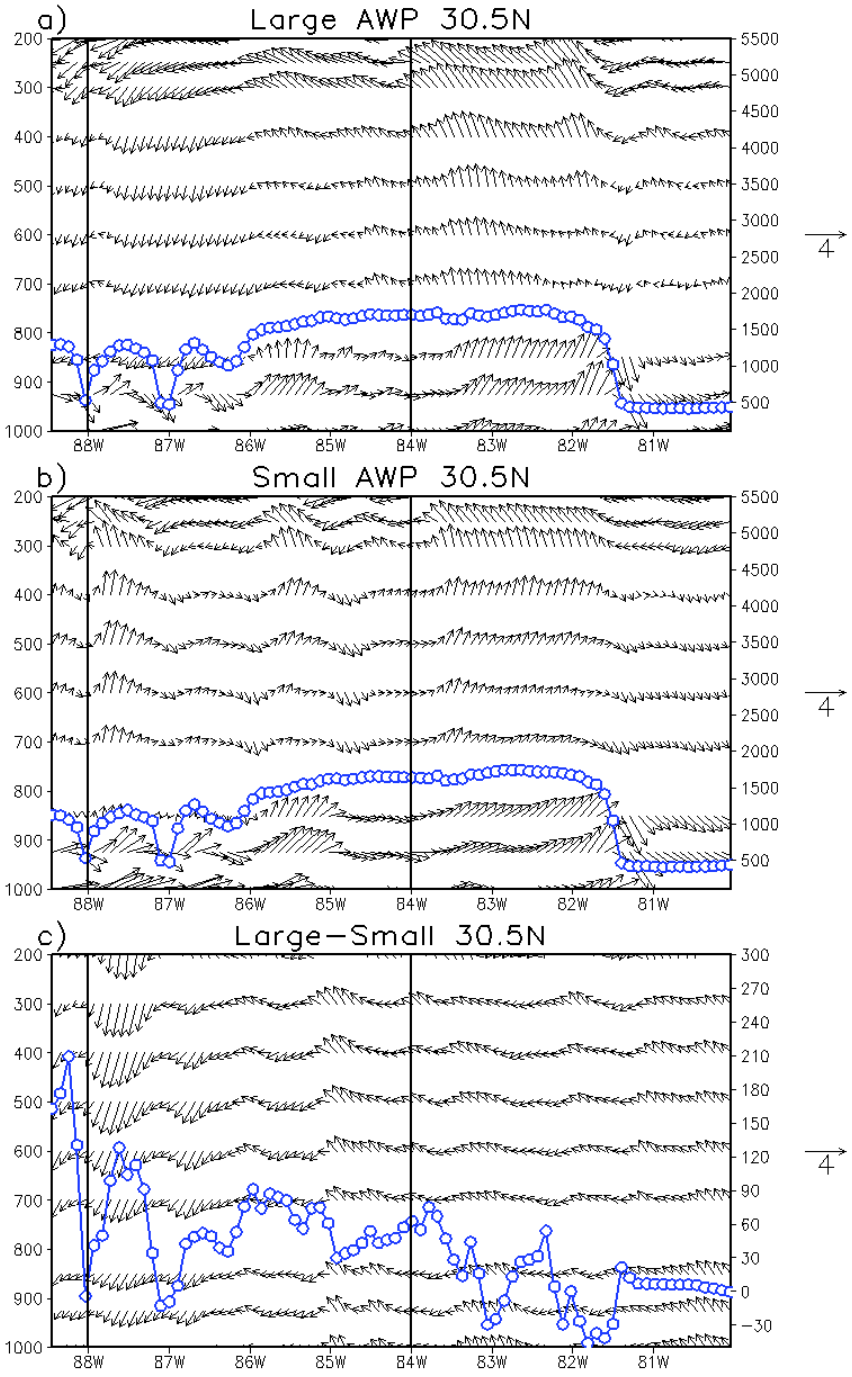

Fig. 3.13. Same as Fig. 3.12 except the variables are from the CLARReS1.0/ERA40 model run.

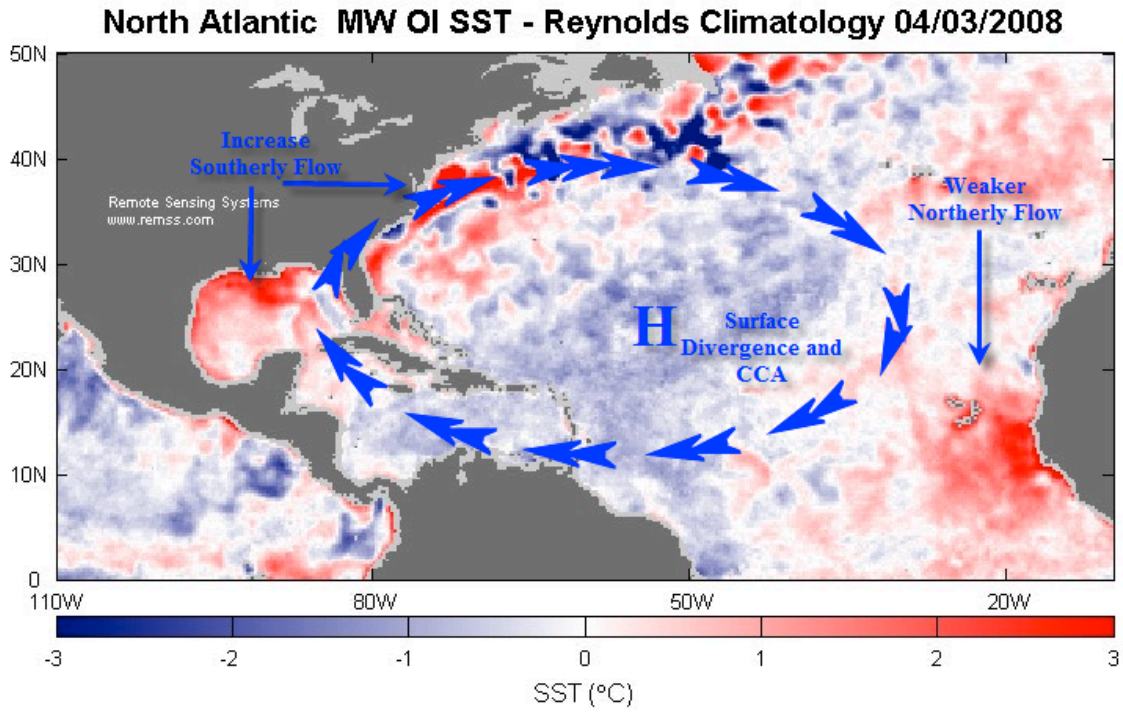

Fig. 3.14. A schematic showing the location of the North Atlantic subtropical high (NASH), from http://talkingmemphis.com/weatherblog/?p=192. The H represents the location of the NASH, and the blue arrowheads denote the flow around the subtropical high. The shaded colors are the SST departures from the Reynolds Climatology using the Microwave Optimally Interpolated product. Information on this product can be found at http://www.ssmi.com/hurricane/active_storms.html#sst.

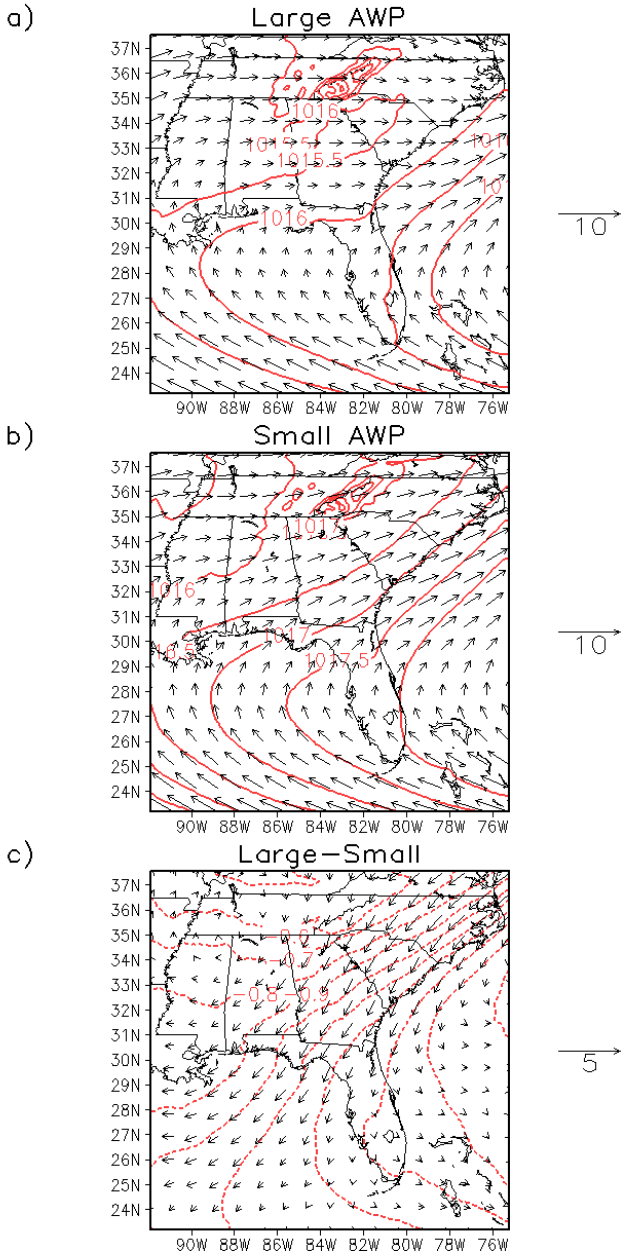

Fig. 3.15. AWP pressure and wind composites. The red contours denote the mean sea level pressure from the CLARReS1.0/R2 model run, in units of hPa. The vectors denote the horizontal flow at 850 hPa, also from the CLARReS1.0/R2 model run, in units of m/s with the scale vector shown by the arrow to the right of the plot. The panels are (a) the large AWP JJA composite mean, (b) the small AWP JJA composite mean and (c) the difference (large-small) between the two composite means.

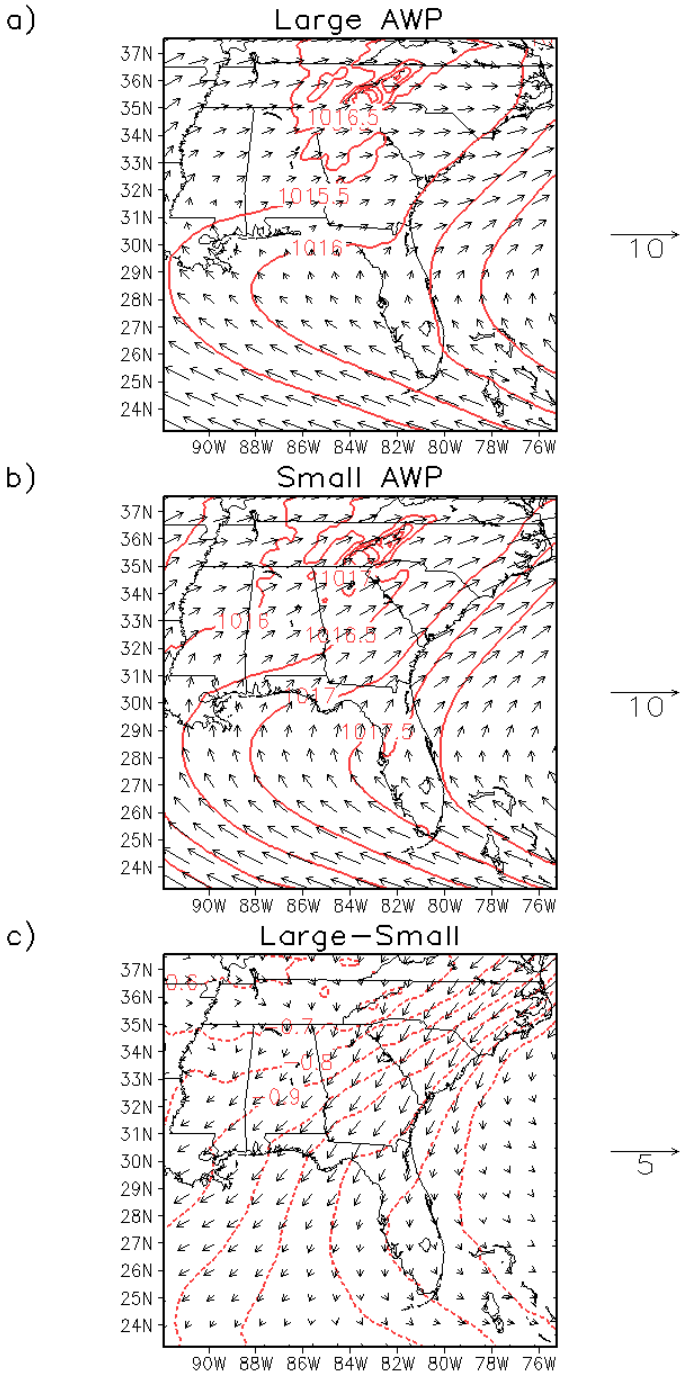

Fig. 3.16. Same as Fig. 3.15 except the variables are from the CLARReS1.0/ERA40 model run.

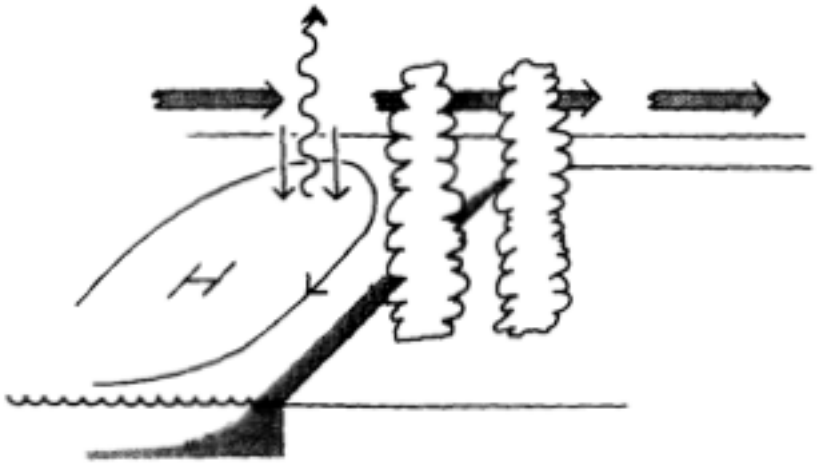

Fig. 3.17. Schematic from Hoskins (1996) showing the Sverdrup vorticity balance in relation to monsoon heating (denoted by puffy clouds), the persistent subtropical high (denoted by H), and flow (denoted by arrows).

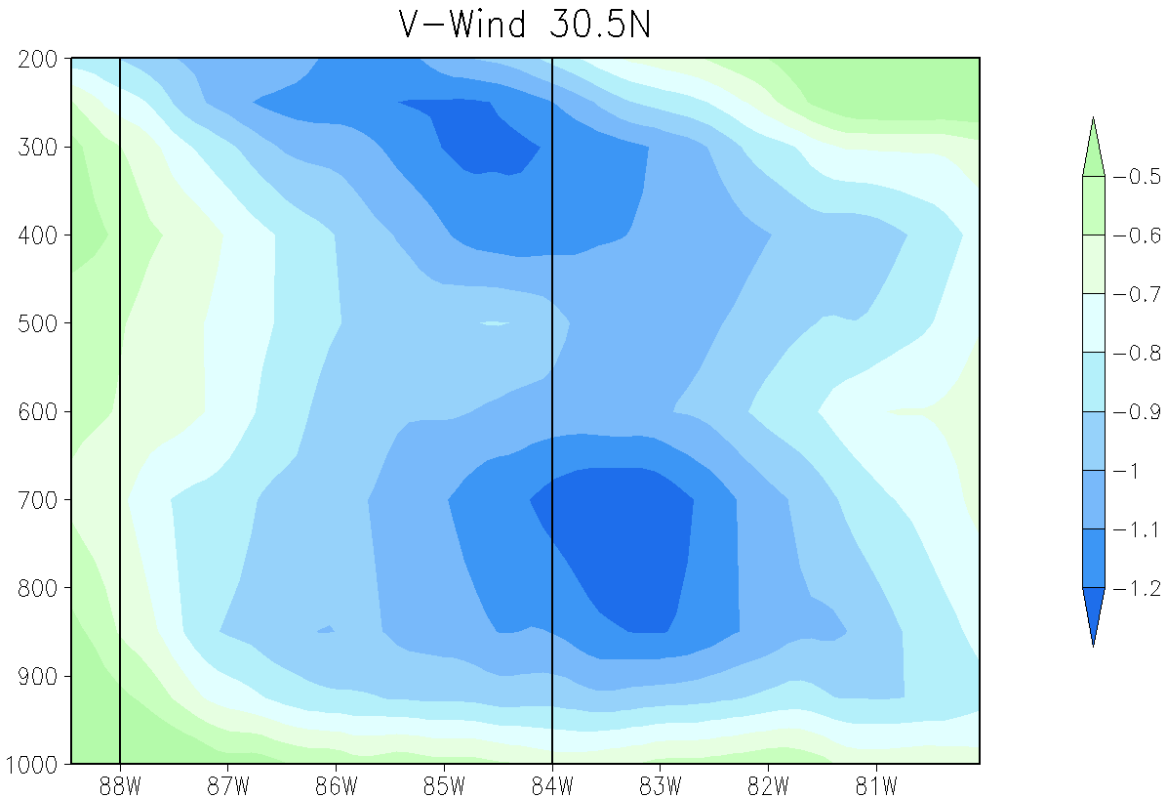

Fig. 3.18. Cross section through 30.5˚N. The black lines denote the locations of longitudes 84˚W and 88˚W. The shading is the meridional flow, in which negative values are equatorward flow, in units of m/s. The wind is from the CLARReS1.0/R2 and is the composite mean difference (large-small) over JJA.

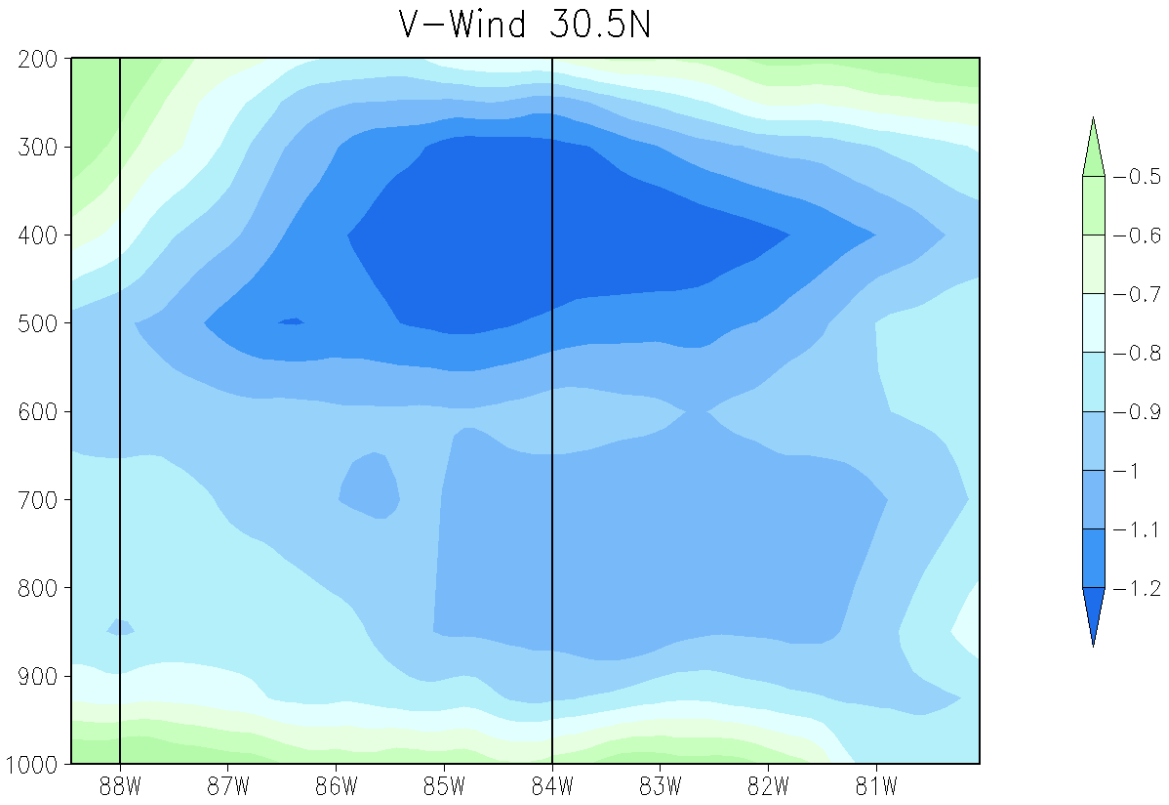

Fig. 3.19. Same as Fig. 3.18 except the data are from the CLARReS1.0/ERA40 model run.

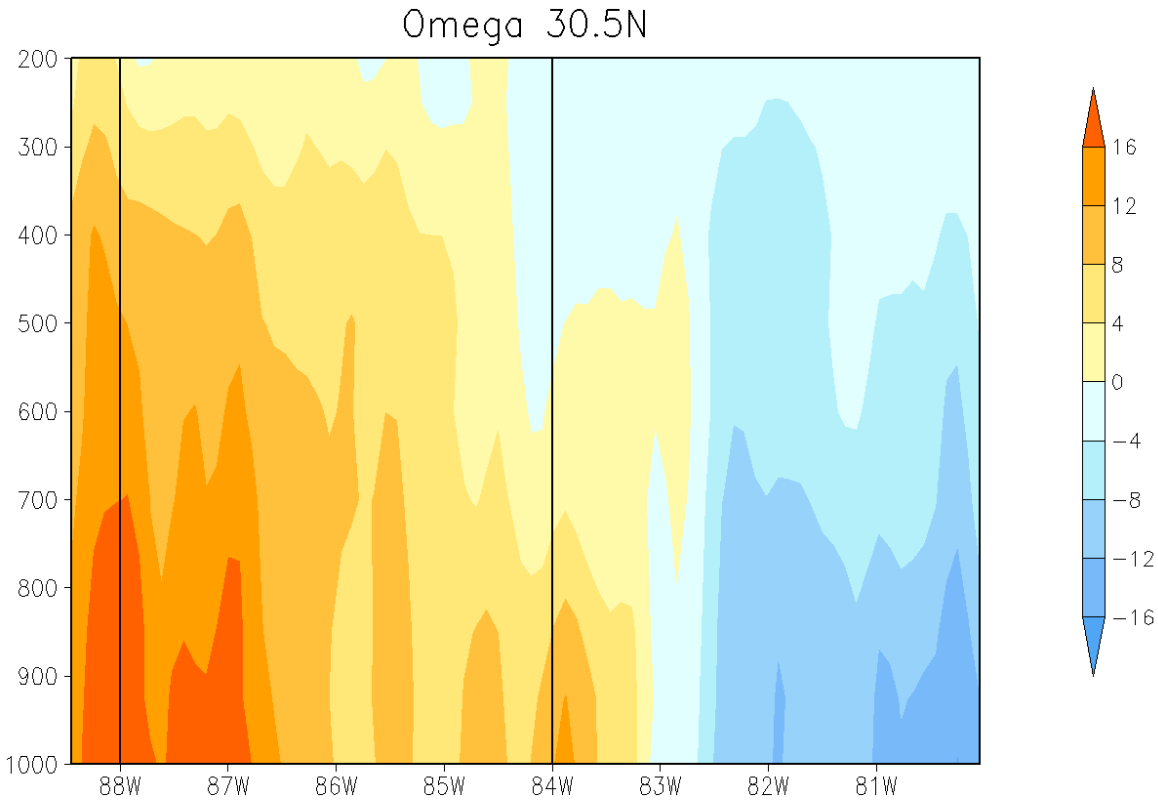

Fig. 3.20. Cross section through 30.5˚N. The black lines denote the locations of longitudes 84˚W and 88˚W. The shading is the vertical velocity in hPa/s; the positive values denote sinking motion. Omega is from the CLARReS1.0/R2. This plot is the composite mean difference (large-small) over JJA.

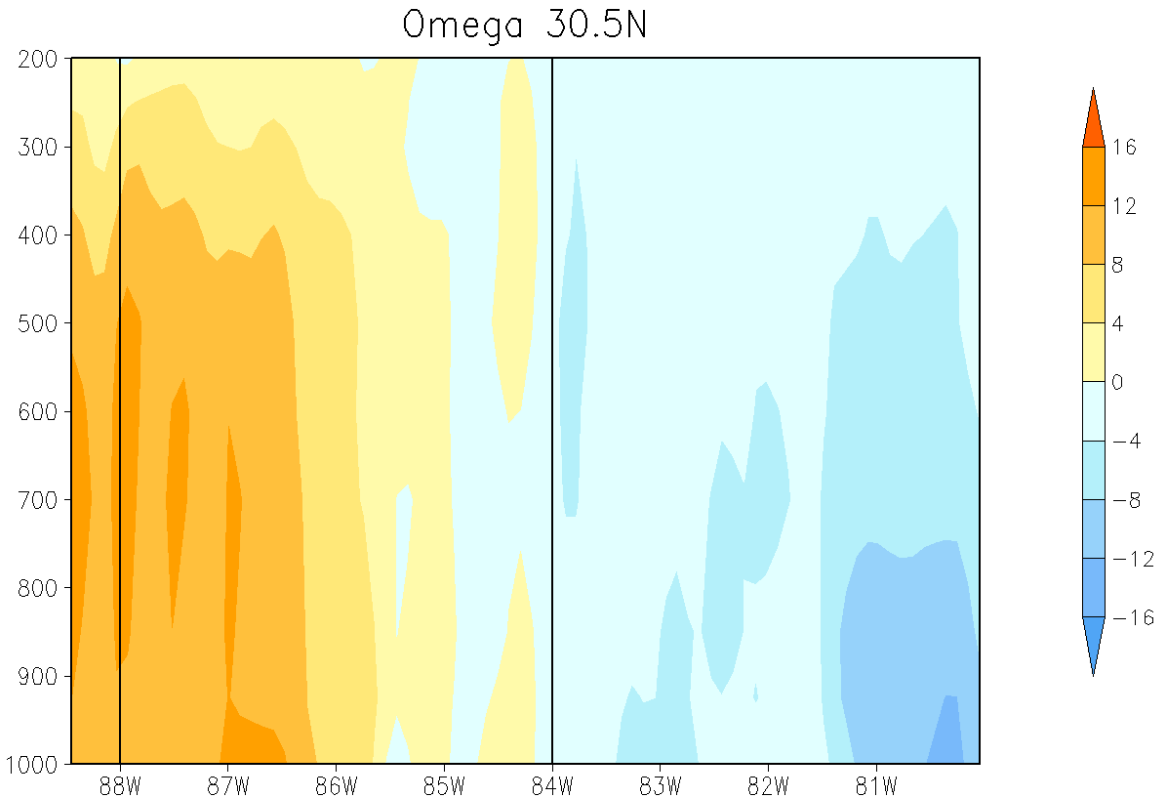

Fig. 3.21. Same as Fig. 3.20 except the data are from the CLARReS1.0/ERA40 model run.

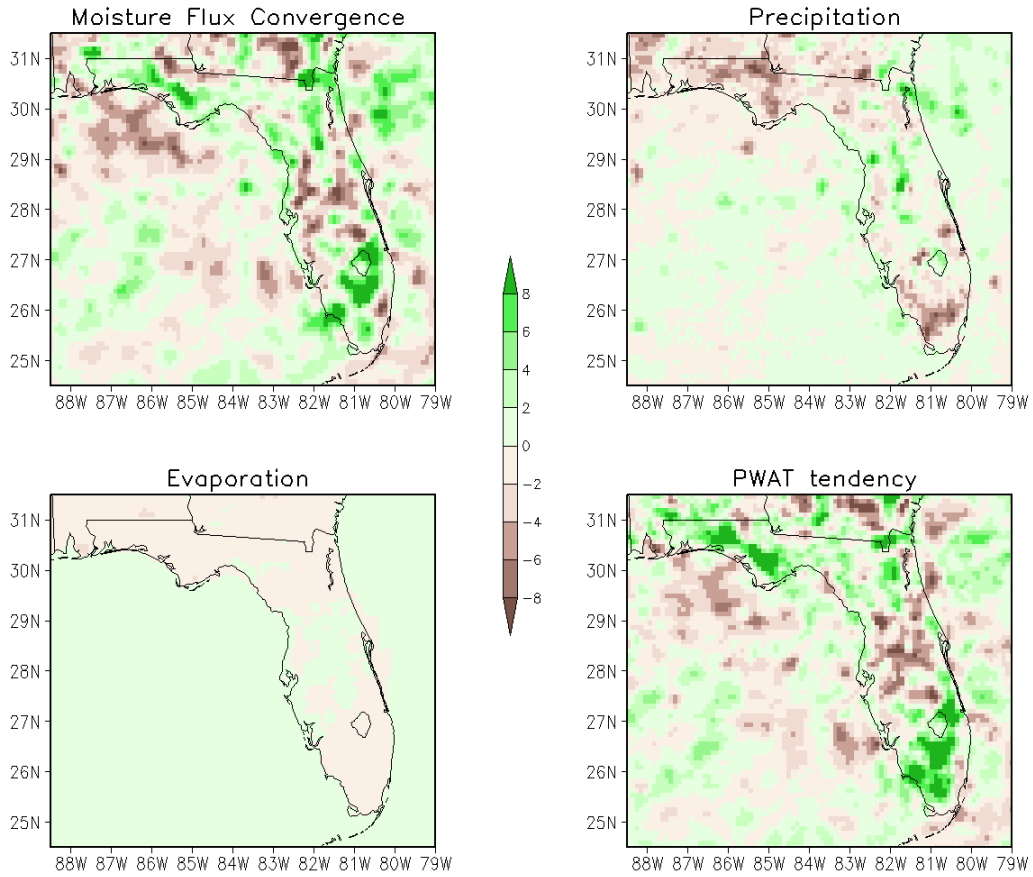

Fig. 3.22. Terms of the moisture budget equations, which are the composite mean difference (large-small) at 4:00 p.m. All are in units of mm day^{-1}. The moisture flux convergence, precipitation and evaporation terms were computed using CLARReS1.0/R2 model run output. The precipitable water tendency is calculated as a residual of these terms.

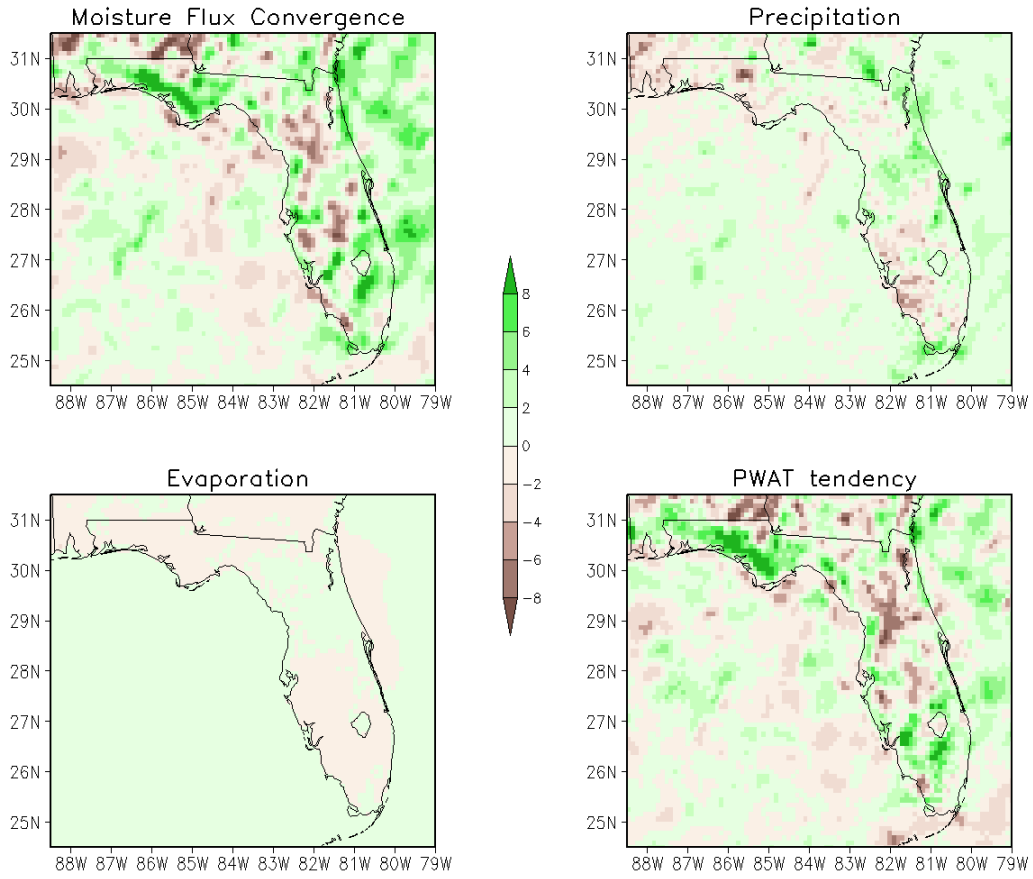

Fig. 3.23. Same as Fig. 3.22 except the variables are from the CLARReS1.0/ERA40 model run.

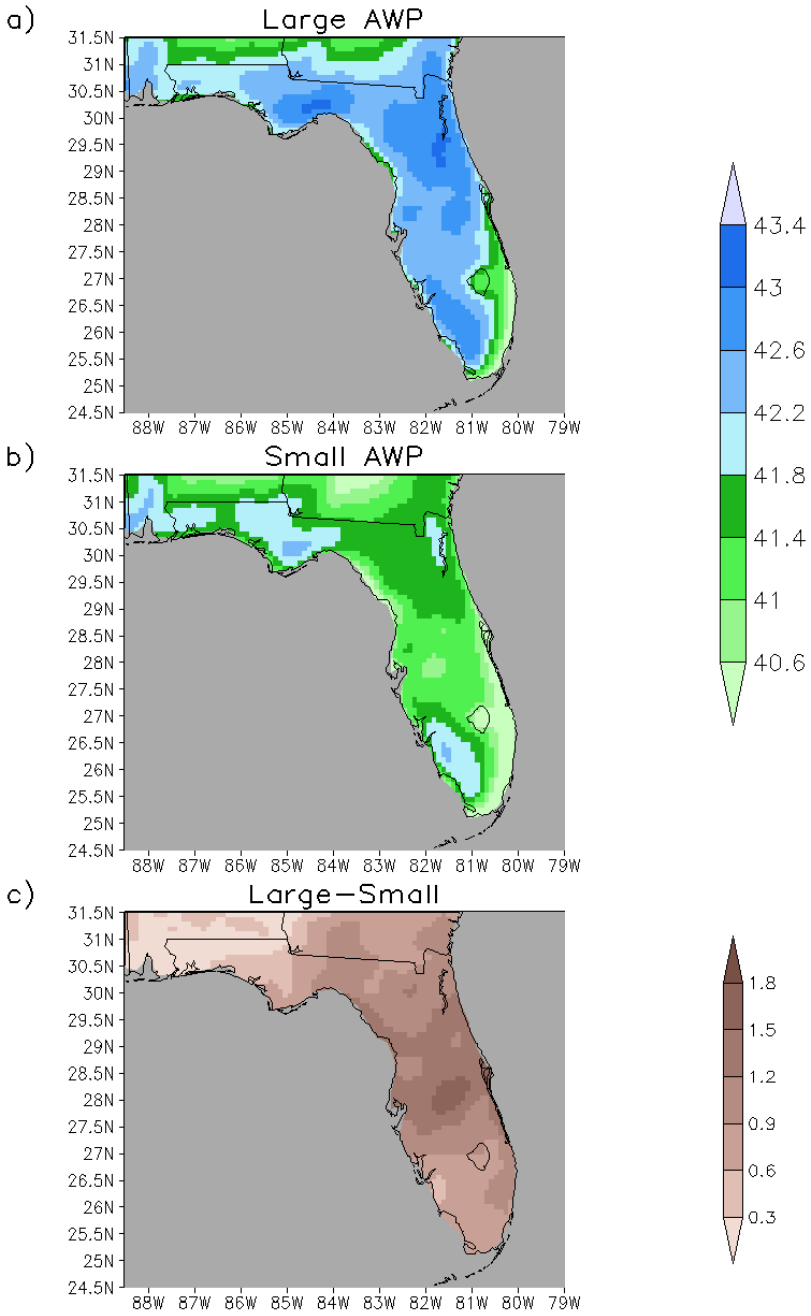

Fig. 3.24. Precipitable water from the CLARReS1.0/R2 model integration for (a) the large AWP JJA composite mean, (b) the small AWP JJA composite mean, and (c) the difference (large-small) between the two composite means. The units are in kg/m^2.

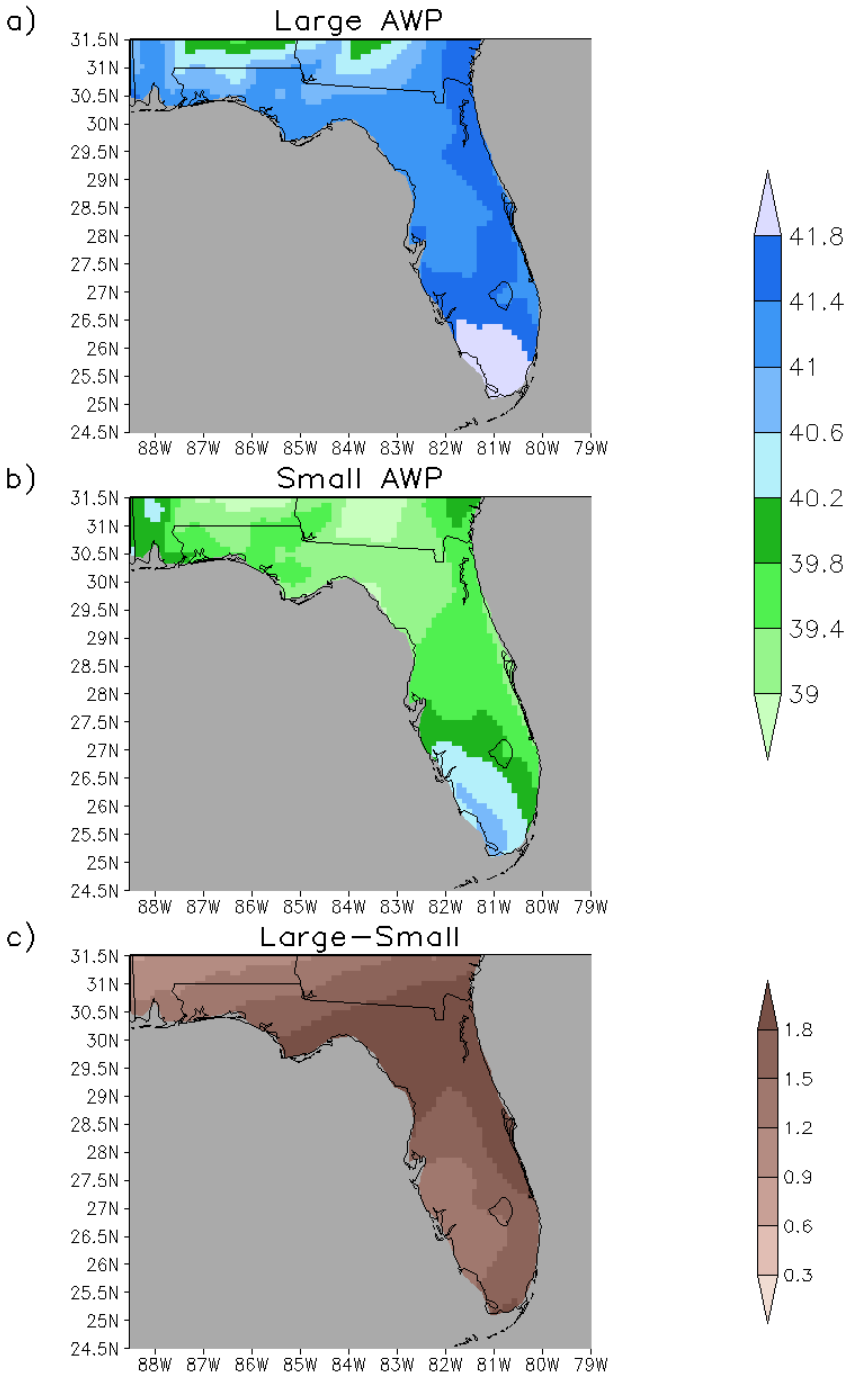

Fig. 3.25. Same as Fig. 3.24 except the data are from the CLARReS1.0/ERA40 model run.

CHAPTER FOUR

CONCLUSIONS

The objective of this study is to determine interannual variations of the sea breeze and convection and to determine the cause of these variations. To accomplish this objective the CLARReS model is created by downscaling both the R2 and ERA-40 reanalyses with the RSM model provided by NCEP-ECPC. During this downscaling process the lateral boundary conditions are forced with atmospheric variables taken from the reanalyses every six hours. Downscaling yields a product with a much finer grid spacing (10-km grid spacing) than either previous reanalysis. Both CLARReS model integrations are compared with two validation datasets to check for reliability. The NCEP-EMC precipitation estimates are available hourly; on the other hand, the CPC precipitation is only available daily. Thus, the NCEP-EMC precipitation is used specifically for the diurnal climatological mean of the precipitation over Florida, and the CPC precipitation is used to check the validity of the interannual output. On the diurnal scale both CLARReS1.0/R2 and CLARReS1.0/ERA40 correctly simulate the times of maximum and minimum precipitation (4:00 p.m. and 4:00 a.m., respectively). The maximum vertical motions are also reproduced at this time close to the coasts, with maximum vertical descent over water and maximum vertical ascent over land. However, both runs underestimate the amount of precipitation occurring climatologically, CLARReS1.0/R2 more so than CLARReS1.0/ERA40. Observations show that precipitation is weaker over most of Florida during large AWP years than during small AWP years. CLARReS1.0/R2 correctly simulates this pattern on an interannual time scale over the panhandle of Florida west of 84°W, but CLARReS1.0/ERA40 does not include this interannual signal until 86°W. Neither model run reproduces the interannual variations found in the observations over peninsular Florida because of the more complicated nature of the sea breeze over this region.

Reasons for the interannual signal are further investigated. Both models agree in suggesting that the temperature gradient between the panhandle of Florida and the Gulf of Mexico is higher during large AWP years than for small years, even though less precipitation occurs during large AWP years. However, because the precipitation patterns at 4:00 p.m. match the composite difference between the interannual variability of precipitation, the model provides

a strong suggestion that the sea breeze is modulated interannually. CLARReS1.0 indicates that this modulation is related to changes in the intensity and location of the NASH, which varies interannually with the AWP. During large AWP years, the NASH weakens and is located farther east than during small AWP years. Therefore an anomalous equatorward flow over the panhandle of Florida is induced; large-scale subsidence occurs during large AWP years as dictated by the Sverdrup vorticity balance. This mechanism is shown in a schematic (Fig. 4.1), with the opposite effect during small AWP years illustrated in Fig. 4.2.

Finally, the moisture budget equation is examined to resolve stronger circulations during large AWP years despite the lack of convection. The moisture flux convergence over the panhandle of Florida is stronger during large AWP years. Also, when each component of the moisture budget equation is plotted, the precipitable water is shown to increase during large AWP years when calculated as a residual. Therefore, the atmospheric column experiences greater moisture accumulation during large AWP years.

These combined results suggest that low-frequency variations in convection associated with the sea breeze over the Florida panhandle are a result of variations in the AWP. This teleconnection in interannual precipitation is associated with NASH changes in location and intensity, which in turn changes the large-scale flow over the southeast United States. However, these results are restricted to the Florida panhandle. The model integrations are not able to correctly simulate the interannual signal over peninsular and northeast Florida, and at this time the interannual signal for these regions are not understood. The entire state of Florida will be considered in future work in which the effects of land use and land cover on the sea breeze over the model domain will be examined.

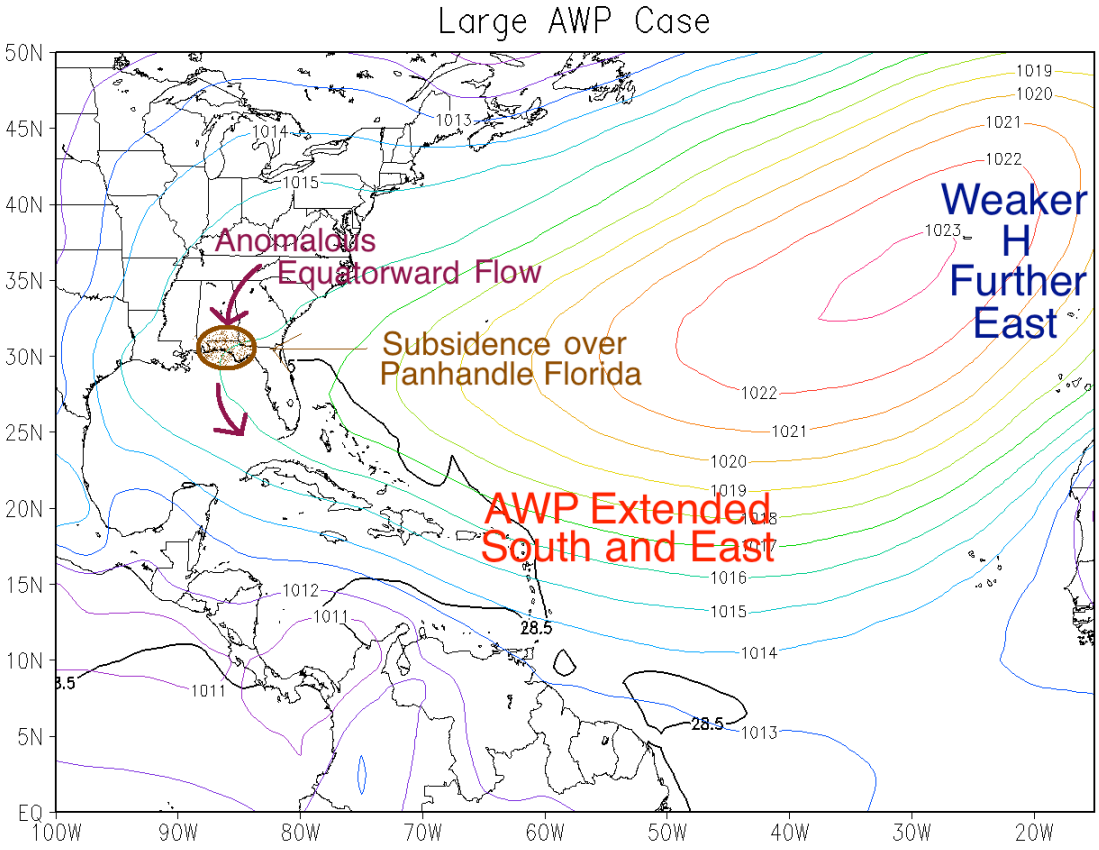

Fig. 4.1. Schematic showing how the AWP affects the low-frequency variance of the panhandle Florida sea breeze for large AWP cases. The rainbow contour lines are mean sea level pressure in hPa. The black contour line denotes the 28.5°C SST isotherm. The maroon arrows depicts the anomalous meridional flow over the southeast United States, and the area of brown stippling shows the area of subsidence.

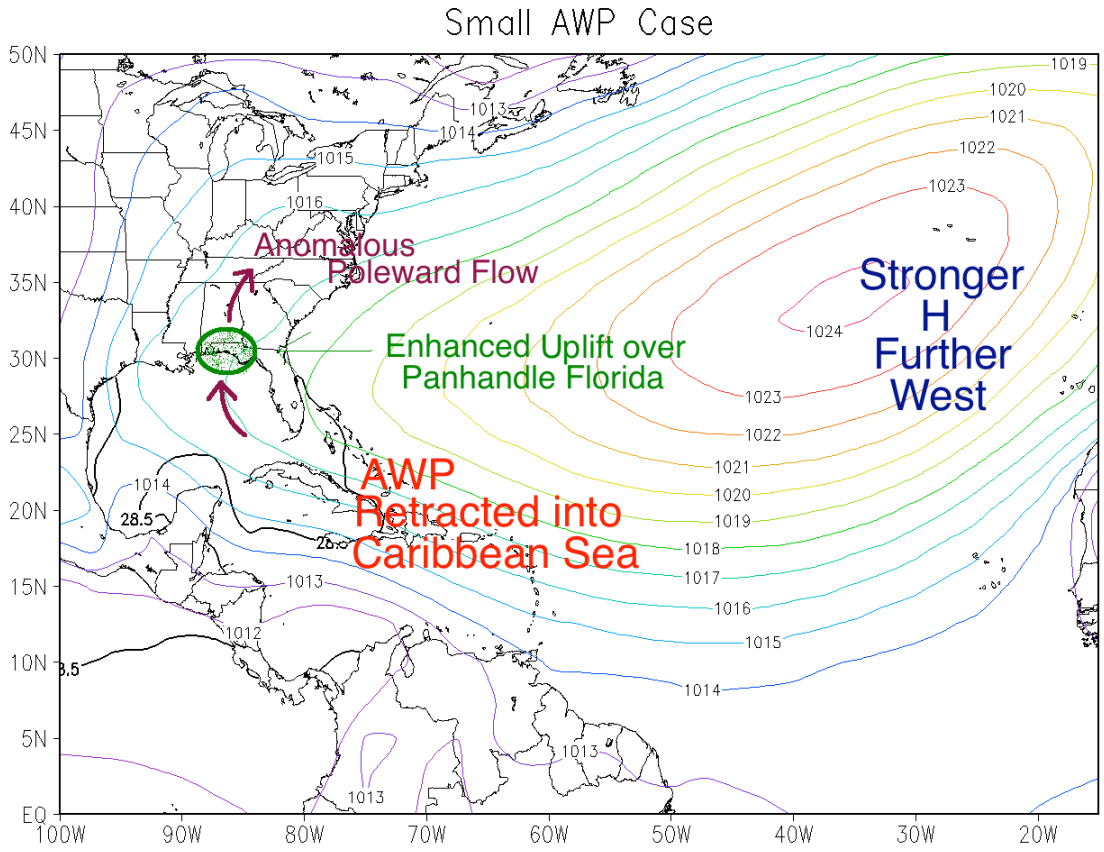

Fig. 4.2. Schematic showing how the AWP affects the low-frequency variance of the panhandle Florida sea breeze for small AWP cases. The rainbow contour lines are mean sea level pressure in hPa. The black contour line denotes the 28.5°C SST isotherm. The maroon arrows depicts the anomalous meridional flow over the southeast United States, and the area of green stippling shows the area of enhanced uplift.

REFERENCES

Arritt, R.W., 1993: Effects of the large-scale flow on characteristic features of the sea breeze. *J. Appl. Meteor.*, 32, 116-125.

Biggs, W.G., and M.E. Graves, 1962: A lake breeze index. *J. Appl. Meteor.*, 1, 474-480.

Carter, L.M., 2003: US National Assessment of the Potential Consequences of Climate Variability and Change Educations Resources Regional Paper: The Southeast. Available online at www.usgcrp.gov/usgcrp/nacc/education/southeast/se-edu-3.htm

Chou, M.D. and M. J. Suarez, 1994: An efficient thermal infrared radiation parameterization for use in General Circulation Models. Technical Report Series on Global Modeling and Data Assimilation, National Aeronautical and Space Administration/TM-1994-104606, 3, 85 pp.

Chou, M.D., and K.T. Lee, 1996: Parameterizations for the Absorption of Solar Radiation by Water Vapor and Ozone. J. Atmos. Sci., 53, 1203–1208.

Ek, M. B., K. E. Mitchell, Y. Lin, E. Rogers, P. Grunmann, V. Koren, G. Gayno, and J. D. Tarpley (2003), Implementation of Noah land surface model advances in the National Centers for Environmental Prediction operational mesoscale Eta model, J. Geophys. Res., 108, D228851, doi:10.1029/2002JD003296

Estoque, M.A., 1962: The sea breeze as a function of the prevailing synoptic situation. *J. Atmos. Sci.*, 19, 244-250.

Fuelberg, H.E., and D.G. Biggar, 1994: The preconvective environment of summer thunderstorms over the Florida panhandle. *Weather and Forecasting*, 9, 316-326.

Higgins, R. W., W. Shi, E. Yarosh, and R. Joyce, 2000: Improved United States Precipitation Quality Control System and Analysis. NCEP/Climate Prediction Center Atlas 7, NOAA, 40pp.

Hong, S.Y., and H.L. Pan, 1996: Nonlocal Boundary Layer Vertical Diffusion in a Medium-Range Forecast Model. Mon. Wea. Rev., 124, 2322–2339.

Hoskins, B. (1996): On the existence and strength of the summer subtropical anticyclones, *Bull. Amer. Meteor. Sac.,* 77: 1287-1292.

Hsu, S-A., 1970: Coastal air-circulation system: Observations and empirical model. *Monthly Weather Review*, 98, 487-509.

Juang, H. H., and M. Kanamitsu, 1994: The NMC Nested Regional Spectral Model. Mon. Wea. Rev. 122, 3-26.

Kanamaru, H., and M. Kanamitsu, 2007: Scale-selective bias correction in a downscaling of global analysis using a regional model. *Mon. Wea. Rev.*, **135,** 334–350

Kanamitsu, M., W. Ebisuzaki, J. Woolen, S. K. Yang, J. J. Hnilo, M. Fiorino and J. Potter, 2002: NCEP/DOE AMIP-II Reanalysis (R-2). Bull. Amer. Met. Soc. 83, 1631-1643. DOI: 10.1175/BAMS-83-11-163

Li, W., L. Li, R. Fu, Y. Deng, and H. Wang, 2011: Changes to the North Atlantic Subtropical High and Its Role in the Intensification of Summer Rainfall Variability in the Southeastern United States. *Mon. Wea. Rev.,* under review

Lim, Y.-K., L. B. Stefanova, S. C. Chan, S. D. Schubert, and J. J. O'Brien, 2010: High-resolution subtropical summer precipitation derived from dynamical downscaling of the NCEP/DOE reanalysis: How much small-scale information is added by a regional model? Clim Dyn., doi: 10.1007/s00382-010-0891-2.

Lin, Y., and K. E. Mitchell, 2005: The NCEP stage II/IV hourly precipitation analyses: development and applications. Preprints, 19th Conf. on Hydrology, American Meteorological Society, San Diego, CA, 9-13 January, Paper 1.2.

Lopez, R.E., P.T. Gannon Sr, D.O. Blanchard, and C.C. Balch, 1984: Synoptic and regional circulation parameters associated with a degree of convective shower activity in south Florida. *Monthly Weather Review*, 112, 686-703.

Loveland, T. R., Merchant, J. W., Reed, B. C., Brown, J. F., Ohlen, D. O., Olson, P., and Hutchinson, J., 1995, Seasonal land cover regions of the United States. Annals of the Association of American Geographers, 85, 339–355.

Mak, K-M, and J.E. Walsh, 1976: On the relative intensities of sea and land breezes. *J. Atmos. Sci.*, 33, 242-251.

Miller, S.K. and B.D. Keim, 2003: Synoptic-scale controls on the sea breeze of the central New England coast. *Weather and Forecasting*, 18, 2, 236-248.

Neumann, J. and Y. Mahrer, 1971: A theoretical study of the land and sea breeze circulation. *J. Atmos. Sci.*, 28, 532-542.

Pan, H.-L., and W.-S. Wu, 1994: Implementing a mass-flux convective parameterization package for the NMC Medium Range Forecast Model. Preprints, 10th Conf. on Numerical Weather Prediction, Portland, OR, Amer. Meteor. Soc., 96–98

Pielke, R.A., 1974: A three-dimensional numerical model of the sea-breeze over south Florida. *Monthly Weather Review*, 102, 115-139.

Powell, M. D., and S. K. Rinard, 1998: Marine forecasting at the 1996 centennial Olympic Games. *Wea. Forecasting*, **13,** 764–782.

Rodwell, M. J., and B. J. Hoskins, 2001: Subtropical anticyclones and summer monsoons. J. Climate, 14, 3192–3211.

Simpson, J.E., 1994: Sea Breeze and Local Winds. Cambridge Univ Press, 234 pp.

Slingo, J. M., 1987: The development and verification of a cloud prediction scheme for the ECMWF model. *Quart. J. Roy. Meteor. Soc.,***113,** 899–927

Smith, T. M., R. W. Reynolds, T. C. Peterson, and J. Lawrimore, 2008: Improvements to NOAA's historical merged land-ocean surface temperature analysis (1880-2006). J. Climate, 21, 2283-2296.

Stefanova, L., V. Misra, S. C. Chan, M. Griffin, J. J. O'Brien, and T. J. Smith III, 2011: A proxy for high-resolution regional reanalysis for the Southeast United States. Clim Dyn, under review

Uppala, S. M., and Coauthors, 2005: The ERA-40 reanalysis. *Quart. J. Roy. Meteor. Soc.*, **131,** 2961–3012.

Wang, C. and D. B. Enfield, 2001: The tropical western hemisphere warm pool. Geophys. Res. Lett., 28, 1635-1638.

——, D. B. Enfield, S.-K. Lee, and C. W. Landsea, 2006: Influences of the Atlantic warm pool on Western Hemisphere summer rainfall and Atlantic hurricanes. J. Climate, 19, 3011–3028.

——, and S.-K. Lee, 2007: Atlantic warm pool, Caribbean low- level jet, and their potential impact on Atlantic hurricanes. Geophys. Res. Lett., 34, L02703, doi:10.1029/2006GL028579.

——, S.-K. Lee, and D. B. Enfield, 2008: Climate response to anomalously large and small Atlantic warm pools during the summer. J. Climate, 21, 2437–2450.

Zhou, T., and Coauthors, 2009: Why the western Pacific subtropical high has extended westward since the late 1970s. *J. Climate*, **22,** 2199–2215.

BIOGRAPHICAL SKETCH

Lauren Moeller was born in Washington, Missouri, in 1987. She grew up in a small town on the outskirts of the St. Louis Metropolitan area. When she was 10 her house was hit by a tornado, and at that point she began reading zealously on all types of severe weather phenomenon. This interest led to a decision to pursue meteorology as a career.

After graduating from Warren County R-III, she went to University of Missouri to acquire a Bachelor of Science degree in 2005. While there, Lauren pursued many extracurricular activities. She was a member of the Mizzou Storm Chase team all four years, experiencing three chases. Lauren was also deeply involved in the school's chapter of the AMS/NWA association, and became the first president of the newly established Chi Epsilon Pi Mizzou chapter. Through Chi Epsilon Pi, a tutoring program was started in order to help incoming undergraduates with the course load expected of a meteorology student. Lauren received a research scholarship in 2008, which allowed her to conduct research under the advisement of Dr. Neil Fox. Her topic of research involved the effects of a tree line on evaporation over crop fields. She presented her work in multiple conferences.

Lauren received a Bachelor of Science in Soil, Environmental, and Atmospheric Science in the spring of 2009. She enrolled into Florida State University in fall of 2009 to pursue a Master of Science under the advisement of Dr. Vasubandhu Misra and Dr. James J. O'Brien. She was an active member of the North Florida chapter of the AMS, and won the Member of the Year award for the 2009-2010 year. Lauren was also active in the outreach programs in place at the Center for Oceanic-Atmospheric Prediction Studies, in which she visited elementary and middle school students to teach about weather hazards. She is thankful for all the opportunities given to her at Florida State, and has enjoyed her time there.